

Nonlinear optics of random metal-dielectric films

Vladimir M. Shalaev

Department of Physics, New Mexico State University, Las Cruces, New Mexico 88003

Andrey K. Sarychev

Center for Applied Problems of Electrodynamics, Izhorskaya 13/19, 127412 Moscow, Russia

(Received 16 May 1997; revised manuscript received 8 December 1997)

Surface-enhanced optical nonlinearities are studied in a semicontinuous film consisting of metal granules randomly distributed on an insulating substrate. The local fields are very inhomogeneous in such films and consist of strongly localized sharp peaks. In peaks ("hot" spots), the local fields exceed the applied field by several orders of magnitudes resulting in giant enhancements of the optical nonlinearities. Because of such a pattern for the local field distributions, the nonlinear signals are mostly generated from small nanometer-size areas. The corresponding spatial distributions for the generated fields form, in turn, a set of very sharp peaks on a homogeneous, on average, semicontinuous film. It is shown that the spatial positions of the localized hot spots at the fundamental and generated frequencies are located, in general, in different parts of a film. The local enhancements in the hot spots exceed the average enhancement by several orders of magnitude. The predicted giant local enhancements open fascinating possibilities in nonlinear spectroscopy of single molecules on a semicontinuous metal film. A number of surface-enhanced optical nonlinearities are studied, namely, those that are responsible for the Kerr-effect, four-wave mixing, second-, and third-harmonic generation. The enhancement for nonlinear optical processes is shown to strongly increase toward the long-wavelength part of the spectrum. Spatial distributions of the local fields are calculated in our broad-scale numerical simulations. A scaling theory for the high-order field moments is developed. It predicts that the moments of the local fields are very large and independent of the frequency in a wide spectral range. The theory predicts anomalous field fluctuations and giant enhancements for the nonlinear optical processes, from the visible to the far-infrared spectral range. [S0163-1829(98)02220-6]

I. INTRODUCTION

Nonlinear electrical and optical properties of metal-dielectric percolating composites have attracted much attention in recent years. At zero frequency, strong nonlinearity may result in a breaking down of conducting elements when the electric current exceeds some critical value.¹⁻⁴ If the external electric field exceeds some value known as the critical field, a crack spreads over the system. The critical field amplitude decreases to zero when the concentration of the conducting component approaches the percolation threshold. That is, percolating composites become progressively more responsive to the external field as the percolation threshold approaches. This simplest fuse model can be applied, e.g., for a description of fractures in disordered media and the related problem of weak tensility of materials in comparison to the strength of the atomic bonds.⁵ The tension concentrates around weak points of the materials and a crack spreads out starting from these weak points.

Another example of unusual nonlinear behavior has been observed recently for the ac and dc conductivities in a percolating mixture of carbon particles embedded in the wax matrix.⁶ In this case, neither carbon particles nor the wax matrix have any nonlinearity in their conductivities; nevertheless, the conductivity of a macroscopic composite sample increases twice when the applied voltage increases by a few volts. Such a strong nonlinear response can be attributed to the quantum tunneling between conducting (carbon) particles, which is a distinguishing feature of the electric trans-

port in composites near the percolation threshold.⁷ The current and electric field are concentrated in a few "hot" junctions and makes it possible to change their conductances under the action of the high local fields, whereas the external field is relatively small. In general, percolating systems are very sensitive to the external electric field since their transport and optical properties are determined by a rather sparse network of conducting channels, and the field concentrates in the weak points of the channels. Therefore, composite materials should have much larger nonlinear susceptibilities at zero and finite frequencies than those of its constituents.

The distinguishing feature of the percolating composites to amplify nonlinearities of its components have been recognized very early,⁸⁻¹¹ and nonlinear conductivities and dielectric constants have been studied intensively in the last decade (see for a review Refs. 12-14). In this paper, we consider weak nonlinearities when the dependence of conductivity $\sigma(E)$ on the electric field E can be expanded in the series of E and the leading term, i.e., the linear conductivity $\sigma^{(0)}$ is much larger than the others. This situation is typical for the various nonlinearities in optical and infrared spectral ranges considered here. Even weak nonlinearities lead to qualitatively new physical effects. For example, the generation of higher harmonics can be greatly enhanced in percolating composites, the bistable behavior of the effective conductivity can take place when the conductivity switches between two stable values, etc.¹⁵

The local field fluctuations can be strongly enlarged in the optical and infrared spectral ranges for a composite material

containing metal particles that are characterized by the dielectric constant with negative real and small imaginary parts. Then the enhancement is due to the plasmon resonance in the metallic granules.^{12,14,16,17} The strong fluctuations of the local electric field lead to a corresponding enhancement of various nonlinear effects. Nonlinear percolating composites are potentially of great practical importance¹⁸ as media with intensity-dependent dielectric functions and, in particular, as nonlinear filters and optical bistable elements. The optical response of the nonlinear composites can be tuned by controlling the volume fraction and morphology of constituents.

A special class of metal-dielectric nanocomposites are those with a fractal distribution of metal particles in the composite. In Refs. 10,19–21, nonlinear optical properties of fractal aggregates have been studied. The main result is that the aggregation of initially isolated particles into fractals results in a huge enhancement of the nonlinear response within the spectral range of the cluster plasmon resonances. The typical size $a_0 \sim 10$ nm of metal particles in fractal clusters is much smaller than the wavelength $\lambda > 300$ nm in the optical and infrared spectral ranges. The average density of the particles in fractals is much smaller than in bulk materials and tends to zero with increasing fractal size. With these simplifications, it is possible to consider each particle as an elementary dipole and introduce corresponding interaction operators. Then the problem of the optical response of metal fractals reduces to diagonalizing the interaction operator of the dipoles induced by light. Local fields fluctuations in metal fractals were studied in Refs. 22,23. It has been found that the areas of large field fluctuations are localized in different small parts of a fractal that change with the wavelength.

The prediction of large enhancements of optical nonlinearities in the metal fractals was confirmed experimentally for the example of degenerate four-wave mixing and nonlinear refraction and absorption.¹⁹ Aggregation of initially isolated silver particles into fractal clusters in these experiments led to a 10^6 -fold enhancement of the efficiency of the nonlinear four-wave process and $\sim 10^3$ enhanced nonlinear refraction and absorption. The localized and strongly fluctuating local fields in fractals were imaged by means of the near-field scanning optical microscopy (NSOM) in Ref. 23. A similar pattern for the field distribution was obtained for self-affine thin films²⁴ that have a fractal structure of the surface, with different scaling properties in the plane of the film and normal to it.

Enhanced optical processes in composites with a layered structure were studied by Sipe, Boyd, and their co-workers²⁵ both theoretically and experimentally. The theoretical treatment of nonlinear effects in composite with parallel slabs microstructure can be performed analytically due to the rather simple geometry of the system (see also, Ref. 15). Nonlinear susceptibilities of some hierarchical structures and periodic composites with shell structure were considered in Refs. 26 and 27, respectively.

In contrast to fractal and layered systems, the local field distribution and corresponding nonlinearities are poorly known for percolating metal-dielectric composites in the most interesting spectral range where the plasmon resonances occur in metal grains. When a small volume concen-

tration $p \ll 1$ of the nonlinear material is embedded in a linear host the effective nonlinear response of the whole composite can be calculated explicitly.^{28,29} As one would expect the nonlinearities are enhanced at frequency ω_r corresponding to the plasmon resonance of a single metal grain. Numerical calculations³⁰ for a finite concentration p also give a considerable enhancement in the narrow frequency range around ω_r . These calculations also show that the system sizes tractable for the known numerical methods³¹ is not enough to make quantitative conclusions about the nonlinear properties for the frequencies ω close to the resonance frequency ω_r . Our results reported below are qualitatively different from those of Stroud and Zhang.³⁰ We show that the enhancement of the nonlinearities in percolating metal-dielectric composites are by several orders of magnitude larger than in Ref. 30. Moreover, the enhancement occurs not only for $\omega \approx \omega_r$ but it includes the wide frequency range $\omega_r \geq \omega > 1/\tau$, where τ is the relaxation time for the metal conductivity. This frequency range corresponds for silver particles, for example, to the optical, infrared, and far-infrared spectral ranges. This discrepancy may be associated with the rather moderate size of the system $L = 10$ in the calculations of Ref. 30, whereas the local field fluctuations typically have a much larger spatial separation ξ_e for the frequencies $\omega < \omega_r$.^{32–36} Then the system size L is an artificial damping factor that cuts off all field fluctuations with $\xi_e > L$ and results in the corresponding decrease of the nonlinearities.

To avoid direct numerical calculations, the effective medium theory³⁷ that has the virtue of relative mathematical and conceptual simplicity, was extended for the nonlinear response of percolating composites^{13,38–43} and fractal clusters.⁴⁴ For linear problems, predictions of the effective medium theory are usually sensible physically and offer quick insight into problems that are difficult to attack by other means.¹² The effective medium theory, however, has disadvantages typical for all mean-field theories, namely, it diminishes the fluctuations in the system. For example, it assumes that local electric fields have the same volume occupied by each component of the composite. The electric fields in different components are determined self-consistently.

For the static case, the results of the last modification of the nonlinear effective medium theory^{42,43} are in best agreement with comprehensive computer simulations performed for a two-dimensional (2D) percolating composite.^{40,42,43} In spite of this success, the application of any kind of nonlinear effective medium theory is rather questionable for the frequency range corresponding to the plasmon resonance in metal grains. The first theoretical^{33,34,36} and experimental³⁵ results for the field distribution in percolating composites show that the local field distributions contain sharp peaks with distances between them much larger than the metal grain size. This pattern agrees qualitatively with that in the metal fractals^{22,23} and self-affine films.²⁴ Therefore, the local electric field cannot be considered by any means as the same in all metal grains of the composite. Then the main assumption of the effective medium theory fails for the frequency range corresponding to the plasmon resonance in the films.

In the present paper we consider in detail the field spatial distributions and various weak nonlinear effects in random metal-dielectric films (also referred to throughout the text as

semicontinuous metal films). We focus on the optical and infrared spectral ranges where the plasmon resonances are effective in the films.

A semicontinuous metal film can be viewed as a two-dimensional composite material. Semicontinuous metal films can be produced by thermal evaporation or sputtering of metal onto an insulating substrate. In the growing process, first, small metallic grains are formed on the substrate. A typical size a_0 of a metal grain is about $a_0 = 5 - 20$ nm. As the film grows, the metal filling factor increases and coalescences occur, so that irregularly shaped clusters are formed on the substrate eventually resulting in 2D self-similar fractal structures. The concept of self-similarity plays an important role in the description of various properties of the percolating systems.^{17,45,46} It will be used below in the scaling analysis of the field fluctuations. The sizes of the fractal structures diverge in the vicinity of the percolation threshold. A percolating cluster of metal is eventually formed, when a continuous conducting path appears between the ends of a sample. This point is known as the percolation threshold.⁴⁶ The metal-insulator transition is very close to this point, even in the presence of quantum tunneling. At higher surface coverages, the film is mostly metallic, with voids of irregular shape. With further coverage increase, the film becomes uniform.

The optical properties of metal-dielectric films show anomalous phenomena that are absent for bulk metal and dielectric components. For example, the anomalous absorption in the near-infrared spectral range leads to an anomalous behavior of the transmittance and reflectance. Typically, the transmittance is much higher than that of continuous metal films, whereas the reflectance is much lower (see Refs. 12,16,17,47–49, and references therein). Near the percolation threshold, the anomalous absorptance can be as high as 50%.^{35,48,50–52} A number of effective-medium theories were proposed for the calculation of the optical properties of semicontinuous random films, including the Maxwell-Garnett⁵³ and Bruggeman³⁷ approaches and their various modifications.^{12,48,49} The renormalization group method is also widely used to calculate the effective dielectric response of 2D percolating films near the percolation threshold (see Refs. 54–56, and references therein). Recently, a theory based on the direct solution of the Maxwell equations has been suggested.^{35,57} This new theory allows one to *quantitatively* describe the anomalous absorption and other effective optical properties of semicontinuous films.

Some properties of the local field fluctuations in semicontinuous metal films have been considered theoretically^{32–34,36} in the quasistatic approximation. The giant field fluctuations in semicontinuous metal films were directly imaged in Ref. 35. This experiment has been performed for the microwave frequency range using an original microprobe method. It is interesting to note that the structure of the near field fluctuations appears to be similar to that observed in the metal fractals²³ and rough surfaces⁵⁸ in the optical spectral range by using near-field scanning optical microscopy. As now well known, large field fluctuations are responsible, in particular, for surface-enhanced Raman scattering.^{14,21,34,36,59,60}

If the skin effect in metal grains is small, a semicontinuous film can be considered as a 2D object. Then in the optical spectral range where the frequency ω is much larger than

the relaxation rate $\omega_\tau = \tau^{-1}$, a semicontinuous metal film can be modeled as a 2D $L-R-C$ lattice.^{12,17,61} The capacitance C stands for the gaps between metal grains that are filled by dielectric material (substrate) with the dielectric constant ε_d . The inductive elements $L-R$ represent the metallic grains that for the Drude metal are characterized by the following dielectric function:

$$\varepsilon_m(\omega) = \varepsilon_b - (\omega_p/\omega)^2/[1 + i\omega_\tau/\omega], \quad (1)$$

where ε_b is a contribution to ε_m due to the interband transitions, ω_p is the plasma frequency, and $\omega_\tau = 1/\tau \ll \omega_p$ is the relaxation rate. In the high-frequency range considered here, losses in metal grains are small, $\omega_\tau \ll \omega$. Therefore, the real part of the metal dielectric function is much larger (in modulus) than the imaginary part and it is negative for frequencies ω less than the renormalized plasma frequency

$$\omega_p^* \cong \omega_p / \sqrt{\varepsilon_b}. \quad (2)$$

Thus the metal conductivity is almost purely imaginary and metal grains can be modeled as $L-R$ elements, with the active component much smaller than the reactive one.

If the skin-effect cannot be neglected, i.e., the skin depth δ is smaller than the metal grain size a_0 , the simple quasistatic description of a semicontinuous film as a 2D array of the $L-R$ and C elements is not valid. Still we can use the $L-R-C$ model in the other limiting case, when the skin effect is very strong, $\delta \ll a_0$.⁵⁷ In this case, losses in metal grains are small, regardless of the ratio ω/ω_τ , whereas the effective inductance for a metal grain depends on the grain size and shape rather than on the material constants for the metal. Such a system has been studied in the recent experiment found in Ref. 35.

It is instructive to consider first the film properties at the percolation threshold $p = p_c$, where the exact Dykhne result for the effective dielectric constant $\varepsilon_e = \sqrt{\varepsilon_d \varepsilon_m}$ (Ref. 62) holds in the quasistatic case. If we neglect the metal losses and put $\omega_\tau = 0$, the metal dielectric constant ε_m is negative for frequencies smaller than the renormalized plasma frequency ω_p^* . We also neglect possible small losses in a dielectric substrate, assuming that ε_d is real and positive. Then, ε_e is purely imaginary for $\omega < \omega_p^*$. Therefore, a film consisting of loss-free metal and dielectric grains is absorptive, for $\omega < \omega_p^*$. The effective absorption in a loss-free film means that the electromagnetic energy is stored in the system and thus the local fields could increase unlimitedly. In reality, the local fields in a metal film are, of course, finite because of the losses. If the losses are small, one anticipates very strong field fluctuations. These large fluctuations may result in giant enhancements of optical nonlinearities.^{12,14}

In this paper, we study surface-enhanced optical nonlinearities of semicontinuous metal films. The paper is organized as follows. In Sec. II, we briefly recapitulate the approach developed in Refs. 32–34 for calculating local fields in a semicontinuous film. We describe here the numerical recipe used and show results of our calculations for local field distributions. We show that the local field distributions consist of very sharp peaks that in some cases are correlated in space. We also consider here dependencies of the field distributions on the light wavelength and metal concentration. In Sec. III, we present the scaling theory that describes

the field distributions and their dependencies on the wavelength and metal concentration. The theory allows one to estimate enhancements of different nonlinearities. In Sec. IV, we derive the formalism and calculate numerically the surface-enhanced optical nonlinearities for a number of optical processes, namely, nonlinear refraction and absorption associated with the Kerr-type nonlinear susceptibilities, four-wave mixing, second-, and third-harmonic generation. For all these processes, we calculate spatial local distributions of the enhanced optical nonlinearities on a metal semicontinuous film. A distinctive feature of these distributions is that most of the enhancement occurs in strongly localized nanometer-scale areas. The enhancement in these ‘‘hot zones’’ is giant and exceeds a ‘‘background’’ nonlinear signal by many orders of magnitude. These effects can be obtained experimentally in the optical range by using, for example, near-field scanning optical microscopy allowing a subwavelength resolution^{23,58,63} and, in the microwave range, by using the subwavelength probe method.³⁵ Concluding discussions are presented in Sec. V.

II. GIANT LOCAL FIELDS ON SEMICONTINUOUS METAL FILMS

A. Linear response

We consider optical properties of a semicontinuous film consisting of metal grains randomly distributed on a dielectric substrate. The film is placed in the $\{x, y\}$ plane, whereas the incident wave propagates in the z direction. The local conductivity $\sigma(\mathbf{r})$ of the film takes either the ‘‘metallic’’ values $\sigma(\mathbf{r}) = \sigma_m$ in metallic grains or the ‘‘dielectric’’ values $\sigma(\mathbf{r}) = -i\omega\varepsilon_d/4\pi$ outside the metallic grains. The vector $\mathbf{r} = \{x, y\}$ has two components in the plane of the film; ω is the frequency of the incident wave. The gaps between metallic grains are assumed to be filled by the material of the substrate, so that the above introduced ε_d is assumed equal to the dielectric constant of the substrate. The electric field in the film is supposed to be homogeneous in direction z perpendicular to the film plane; this means that the skin depth for the metal $\delta \approx c/(\omega\sqrt{\varepsilon_m})$ is much larger than the metal grain size a_0 , and the quasistatic approximation can be applied for calculating the field distributions. We also take into account that the wavelength of the incident wave is much larger than any characteristic size of the film, including the grain size and the gaps between the grains. In this case, the local field $\mathbf{E}(\mathbf{r})$ can be represented as

$$\mathbf{E}(\mathbf{r}) = -\nabla\phi(\mathbf{r}) + \mathbf{E}_e(\mathbf{r}), \quad (3)$$

where $\mathbf{E}_e(\mathbf{r})$ is the applied (macroscopic) field and $\phi(\mathbf{r})$ is the potential of the fluctuating field inside the film. The current density $\mathbf{j}(\mathbf{r})$ at point \mathbf{r} is given by Ohm’s law

$$\mathbf{j}(\mathbf{r}) = \sigma(\mathbf{r})[-\nabla\phi(\mathbf{r}) + \mathbf{E}_e(\mathbf{r})]. \quad (4)$$

The current conservation law $\nabla \cdot \mathbf{j}(\mathbf{r}) = 0$ has the following form:

$$\nabla\{\sigma(\mathbf{r})[-\nabla\phi(\mathbf{r}) + \mathbf{E}_e(\mathbf{r})]\} = 0. \quad (5)$$

We solve Eq. (5) to find the fluctuating potential $\phi(\mathbf{r})$ and the local field $\mathbf{E}(\mathbf{r})$ induced in the film by the applied field $\mathbf{E}_e(\mathbf{r})$. When the wavelength of the incident electromagnetic

(em) wave is much larger than all spatial scales in a semicontinuous metal film, the applied field \mathbf{E}_e , i.e., the field of the incident wave, is constant in the film plane $\mathbf{E}_e(\mathbf{r}) = \mathbf{E}^{(0)}$. Provided the local field $\mathbf{E}(\mathbf{r})$ is known the effective conductivity σ_e can be obtained from the definition

$$\langle \mathbf{j}(\mathbf{r}) \rangle = \sigma_e \mathbf{E}^{(0)}, \quad (6)$$

where $\langle \dots \rangle$ denotes the average over the entire film.

The local field $\mathbf{E}(\mathbf{r})$, induced by the applied field $\mathbf{E}_e(\mathbf{r})$, can be obtained by using the nonlocal conductivity \hat{S} introduced in Ref. 34:

$$\mathbf{E}(\mathbf{r}) = \frac{\mathbf{j}(\mathbf{r})}{\sigma(\mathbf{r})} = \frac{1}{\sigma(\mathbf{r})} \int \hat{S}(\mathbf{r}, \mathbf{r}') \mathbf{E}_e(\mathbf{r}') d\mathbf{r}'. \quad (7)$$

According to Eq. (7) the nonlocal conductivity $\hat{S}(\mathbf{r}, \mathbf{r}')$ relates the applied field at point \mathbf{r}' to the current and the local field at point \mathbf{r} . The nonlocal conductivity in Eq. (7) can be expressed in terms of the Green function of Eq. (5):³⁴

$$S_{\alpha\beta}(\mathbf{r}_2, \mathbf{r}_1) = \sigma(\mathbf{r}_2)\sigma(\mathbf{r}_1) \frac{\partial^2 G(\mathbf{r}_2, \mathbf{r}_1)}{\partial r_{2\alpha} \partial r_{1\beta}}, \quad (8)$$

where the Greek indices take values 1 or 2. The Green function is symmetric with respect to the interchange of its arguments $G(\mathbf{r}_1, \mathbf{r}_2) = G(\mathbf{r}_2, \mathbf{r}_1)$; therefore, Eq. (8) implies that the nonlocal conductivity is also symmetric:³⁴

$$S_{\alpha\beta}(\mathbf{r}_1, \mathbf{r}_2) = S_{\beta\alpha}(\mathbf{r}_2, \mathbf{r}_1). \quad (9)$$

The introduced nonlocal conductivity \hat{S} is useful for an analysis of different processes in the system.

Suppose, for example, that the external field applied to the film has the following form:

$$\mathbf{E}_e(\mathbf{r}) = \mathbf{E}^{(0)} + \mathbf{E}_f(\mathbf{r}), \quad (10)$$

where $\mathbf{E}^{(0)}$ is the constant field and field $\mathbf{E}_f(\mathbf{r})$ may arbitrary change over the film but its averaged value $\langle \mathbf{E}_f(\mathbf{r}) \rangle$ is collinear to $\mathbf{E}^{(0)}$. Then the average current density $\langle \mathbf{j} \rangle$ is also collinear to $\mathbf{E}^{(0)}$ in the macroscopically isotropic films considered here. Therefore, the average current can be written as

$$\langle \mathbf{j}(\mathbf{r}) \rangle = \frac{\mathbf{E}^{(0)}}{E^{(0)2}} (\mathbf{E}^{(0)} \cdot \langle \mathbf{j}(\mathbf{r}) \rangle) = \frac{\mathbf{E}^{(0)}}{E^{(0)2}} \frac{1}{A} \int E_\alpha^{(0)} j_\alpha(\mathbf{r}) d\mathbf{r}, \quad (11)$$

where A is the total area of the film, the integration is over the film area and $E^{(0)2} \equiv (\mathbf{E}^{(0)} \cdot \mathbf{E}^{(0)})$. By expressing the current $j_\alpha(\mathbf{r})$ in Eq. (11) in terms of the nonlocal conductivity matrix $j_\alpha(\mathbf{r}) = \int S_{\alpha\beta}(\mathbf{r}, \mathbf{r}_1) E_{e\beta}(\mathbf{r}_1) d\mathbf{r}_1$, we obtain

$$\langle \mathbf{j}(\mathbf{r}) \rangle = \frac{\mathbf{E}^{(0)}}{E^{(0)2}} \frac{1}{A} \int E_\alpha^{(0)} S_{\alpha\beta}(\mathbf{r}, \mathbf{r}_1) E_{e\beta}(\mathbf{r}_1) d\mathbf{r} d\mathbf{r}_1, \quad (12)$$

where the integrations are over the entire film. Now we integrate this equation over the coordinates \mathbf{r} and use the symmetry of the matrix of nonlocal conductivity given by Eq. (9); this results in the expression

$$\langle \mathbf{j}(\mathbf{r}) \rangle = \frac{\mathbf{E}^{(0)}}{E^{(0)2}} \frac{1}{A} \int j_{0\beta}(\mathbf{r}_1) E_{e\beta}(\mathbf{r}_1) d\mathbf{r}_1, \quad (13)$$

where $\mathbf{j}_0(\mathbf{r})$ is the current induced at the coordinate \mathbf{r} by the constant external field $\mathbf{E}^{(0)}$. Now we can substitute in Eq. (13) the external field $\mathbf{E}_e(\mathbf{r})$ from Eq. (10) and integrate over the coordinate \mathbf{r}_1 which gives

$$\langle \mathbf{j}(\mathbf{r}) \rangle = \frac{\mathbf{E}^{(0)}}{E^{(0)2}} (\mathbf{E}^{(0)} \cdot \langle \mathbf{j}_0(\mathbf{r}) \rangle) + \frac{\mathbf{E}^{(0)}}{E^{(0)2}} \langle [\sigma(\mathbf{r}) \mathbf{E}(\mathbf{r}) \cdot \mathbf{E}_f(\mathbf{r})] \rangle, \quad (14)$$

where the field $\mathbf{E}(\mathbf{r}) = \mathbf{j}_0(\mathbf{r})/\sigma(\mathbf{r})$ is the local field induced in the film by the constant external field $\mathbf{E}^{(0)}$. Substituting in Eq. (14) the expression for the effective conductivity given by Eq. (6), we obtain the equation

$$\langle \mathbf{j}(\mathbf{r}) \rangle = \mathbf{E}^{(0)} \left[\sigma_e + \frac{\langle \sigma(\mathbf{r}) [\mathbf{E}(\mathbf{r}) \cdot \mathbf{E}_f(\mathbf{r})] \rangle}{E^{(0)2}} \right]. \quad (15)$$

Thus, the average current induced in a macroscopically isotropic film by a nonuniform external field $\mathbf{E}_e(\mathbf{r})$ can be expressed in terms of the fluctuating part $\mathbf{E}_f(\mathbf{r})$ of the external field and the local field $\mathbf{E}(\mathbf{r})$ induced in the film by the constant part $\mathbf{E}^{(0)}$ of the external field. It is easy to verify that Eq. (15) is invariant with respect to the partition of the external field in the constant and fluctuating parts. Below we will use Eq. (15) in an analysis of the nonlinear response of semicontinuous metal films since it allows one to express various nonlinear currents in terms of the local fields.

Consider, for example, a composite with the local conductivity $\sigma(\mathbf{r})$ including the cubic nonlinearity, i.e., $\sigma(\mathbf{r}) = \sigma^{(0)}(\mathbf{r}) + \sigma^{(3)}(\mathbf{r})|\mathbf{E}(\mathbf{r})|^2$. To find the effective conductivity σ_e (which, of course, is also nonlinear), we write Eq. (5) in the form

$$\nabla \left(\sigma_0(\mathbf{r}) \left[-\nabla \phi(\mathbf{r}) + \mathbf{E}^{(0)} + \frac{\sigma^{(3)}(\mathbf{r})}{\sigma^{(0)}(\mathbf{r})} \mathbf{E}'(\mathbf{r}) |\mathbf{E}'(\mathbf{r})|^2 \right] \right) = 0, \quad (16)$$

where $\mathbf{E}'(\mathbf{r}) = -\nabla \phi(\mathbf{r}) + \mathbf{E}^{(0)}$ is the local electric field at coordinate \mathbf{r} in the nonlinear film, with the local conductivity containing the cubic term. We consider the last term in the square brackets as an external inhomogeneous field and use the above derived Eq. (15) to obtain the average current

$$\langle \mathbf{j}(\mathbf{r}) \rangle = \sigma_e^{(0)} \mathbf{E}^{(0)} + \mathbf{E}^{(0)} \frac{\langle \sigma^{(3)}(\mathbf{r}) [\mathbf{E}(\mathbf{r}) \cdot \mathbf{E}'(\mathbf{r})] |\mathbf{E}'(\mathbf{r})|^2 \rangle}{E^{(0)2}}, \quad (17)$$

where $\sigma_e^{(0)}$ is the effective conductivity and $\mathbf{E}(\mathbf{r})$ is the local field found in the linear approximation [i.e., for the local conductivity $\sigma(\mathbf{r}) \equiv \sigma^{(0)}(\mathbf{r})$]. Equation (17) expresses the average current and, thus, the effective nonlinear conductivity in terms of the local fields $\mathbf{E}'(\mathbf{r})$ and $\mathbf{E}(\mathbf{r})$.

For a weak nonlinearity, when $\sigma^{(3)}(\mathbf{r})|\mathbf{E}(\mathbf{r})|^2 \ll \sigma^{(0)}(\mathbf{r})$, we can replace the local field $\mathbf{E}'(\mathbf{r})$ in Eq. (17) by the field $\mathbf{E}(\mathbf{r})$ calculated in the linear approximation; this gives

$$\langle \mathbf{j}(\mathbf{r}) \rangle = \left(\sigma_e^{(0)} + \frac{\langle \sigma^{(3)}(\mathbf{r}) E^2(\mathbf{r}) |\mathbf{E}(\mathbf{r})|^2 \rangle}{E^{(0)2}} \right) \mathbf{E}^{(0)}, \quad (18)$$

where $E^2(\mathbf{r}) \equiv (\mathbf{E}(\mathbf{r}) \cdot \mathbf{E}(\mathbf{r}))$. From this equation, it follows that the effective nonlinear conductivity σ_e has the form

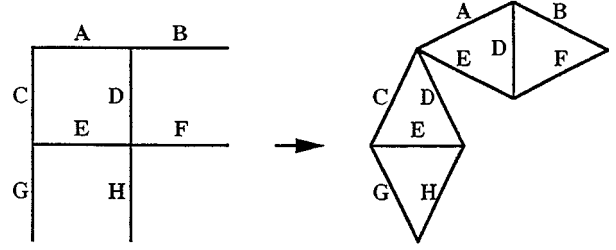


FIG. 1. The real space renormalization scheme.

$$\sigma_e = \sigma_e^{(0)} + \sigma_e^{(3)} |\mathbf{E}^{(0)}|^2, \quad (19)$$

where the effective nonlinear conductivity $\sigma_e^{(3)}$ is equal to

$$\sigma_e^{(3)} = \frac{\langle \sigma^{(3)}(\mathbf{r}) E^2(\mathbf{r}) |\mathbf{E}(\mathbf{r})|^2 \rangle}{E^{(0)2} |\mathbf{E}^{(0)}|^2}. \quad (20)$$

Equation (20) expresses $\sigma_e^{(3)}$ in terms of the local fields $\mathbf{E}(\mathbf{r})$ obtained in the linear approximation.

When the local fields fluctuate strongly over a system, the effective nonlinearity $\sigma_e^{(3)}$ is strongly enhanced in comparison with the average $\langle \sigma^{(3)}(\mathbf{r}) \rangle$. Equation (20) was obtained independently by Stroud and Hui⁹ and by Shalaev *et al.*,¹⁰ and it is widely used in analyses of the nonlinear response of composites.^{12,13}

To calculate the local electric fields in the system we discretize Eq. (5) on a square lattice. The potentials in the sites of the lattice reproduce the local field potentials in a semi-continuous film. The conductivities of the lattice bonds stand for the local film conductivity and take either σ_m or σ_d values. In such a way, the partial differential equation (5) is reduced to a set of Kirchhoff equations that are solved by the method presented in the next subsection. Provided the field distribution is known we can use formulas such as Eq. (15) to calculate the optical nonlinearities. Below, we first describe the numerical procedure used and then results of our numerical simulations for the field distributions.

B. Numerical model

There now exist very efficient numerical methods for calculating the effective conductivity of composite materials (see Refs. 12,17,46,64–66), but they typically do not allow calculations of the field distributions. Here, we use the real space renormalization group (RSRG) method that was suggested by Reynolds *et al.*⁶⁷ and Sarychev⁶⁸ and then extended to study the conductivity⁶⁹ and the permeability of oil reservoirs.⁷⁰ Below, we follow the approach used by Aharony.⁷⁰ This method can be adopted to finding the field distributions in the following way.^{33,34} First, we generate a square lattice of L - R (metal) and C (dielectric) bonds using a random number generator. As seen in Fig. 1, such a lattice can be considered as a set of “corner” elements. Such elements are labeled A–H in Fig. 1. In the first stage of the RSRG procedure, each of these elements is replaced by the two Wheatstone bridges, as shown in Fig. 1. After this transformation, the initial square lattice is converted to another square lattice, with the distance between the sites twice as large and with each bond between the two nearest neighbor-

ing sites being the Wheatstone bridge. Note that there is a one-to-one correspondence between the x bonds in the initial lattice and the x bonds in the x directed bridges of the transformed lattice, as seen in Fig. 1. The same one-to-one correspondence exists also between the y bonds. The transformed lattice is also a square lattice, and we can again apply to it the RSRG transformation. We continue this procedure until the size l of the system is reached. As a result, instead of the initial lattice we have two large Wheatstone bridges in the x and y directions. Each of them has a hierarchical structure consisting of bridges with the sizes from 2 to l . Because the one-to-one correspondence is preserved at each step of the transformation, the correspondence also exists between the elementary bonds of the transformed lattice and the bonds of the initial lattice. After using the RSRG transformation, we apply an external field to the system and solve the Kirchhoff equations to determine the fields and the currents in all the bonds of the transformed lattice. Due to the hierarchical structure of the transformed lattice, these equations can be solved exactly. Then, we use the one-to-one correspondence between the elementary bonds of the transformed lattice and the bonds of the initial square lattice to find the field distributions in the initial lattice as well as its effective conductivity. The number of operations to get the full distributions of the local fields is proportional to l^2 to be compared with l^7 operations needed in the transform-matrix method^{12,31} and l^3 operations needed in the well-known Frank-Lobb algorithm,⁶⁴ which does not provide the field distributions but the effective conductivity only. The RSRG procedure is certainly not exact since the effective connectivity of the transformed system does not repeat exactly the connectivity of the initial square lattice. To check the accuracy of the RSRG, we solved the 2D percolation problem using this method. Namely, we calculated the effective parameters of a two-component composite with the real metallic conductivity σ_m much larger than the real conductivity σ_d of the dielectric component $\sigma_m \gg \sigma_d$. We obtained the percolation threshold $p_c = 0.5$ and the effective conductivity at the percolation threshold that is very close to $\sigma(p_c) = \sqrt{\sigma_m \sigma_d}$. These results coincide with the exact ones for 2D composites.⁶² This is not surprising since the RSRG procedure preserves the self-duality of the initial system. The critical exponents obtained by the RSRG procedure are also close to the known values of the exponents from percolation theory.¹² Therefore, we believe that the numerical method used describes, at least qualitatively, the field distributions on semicontinuous films. Below, using the described numerical procedure, we calculate the local field distributions on a random semicontinuous metal film.

C. Field distributions on semicontinuous metal films

As mentioned, we model the film as a square lattice consisting of metallic bonds with the conductivity $\sigma_m = -i\varepsilon_m \omega / 4\pi$ (L - R bonds) and the concentration p , and dielectric bonds with the conductivity $\sigma_d = -i\varepsilon_d \omega / 4\pi$ and concentration $1 - p$ (C bonds). The applied field $E^{(0)}$ is set to be equal to unity $E^{(0)} = 1$, whereas the local fields inside the system are complex quantities. The dielectric constant of silver grains has the form of Eq. (1) with the interband-transition contribution $\varepsilon_b = 5.0$, the plasma frequency ω_p

$= 9.1$ eV, and the relaxation frequency $\omega_r = 0.021$ eV.⁷¹ Below, we set $\varepsilon_d = 2.2$ typical for a glass. In Fig. 2 we show the field distributions $G(\mathbf{r}) = |E(\mathbf{r})/E^{(0)}|^2$ for the plasmon resonance frequency $\omega = \omega_r$ that corresponds to the condition $\text{Re}[\varepsilon_m(\omega_r)] = -\varepsilon_d$. The value of the frequency ω_r is slightly below the renormalized plasma frequency ω_p^* defined above in Eq. (2). For silver particles the resonance condition fulfilled at wavelength $\lambda \approx 365$ nm. The frequency ω_r gives the resonance of an isolated metal particle. (For a 2D, i.e., z -independent problem, particles can be thought of as infinite in the z direction cylinders that resonate, in the quasistatic approximation, at the frequency $\omega = \omega_r$ corresponding to the condition $\text{Re}[\varepsilon_m(\omega_r)] = -\varepsilon_d$, for the field polarized in the x, y plane.) The results are presented for various metal fractions p . For $p = 0.001$ metal grains practically do not interact, so that all the peaks are almost of the same height and indicate the locations of metal particles. Note that a similar distribution is obtained for $p = 0.999$ when the role of metal particles is played by the dielectric voids. For $p = 0.1$ and, especially, for $p = 0.5$, metal grains form clusters of strongly interacting particles. These clusters resonate at different frequencies (than that for an isolated particle), therefore, for the chosen frequency the field peaks are smaller, on average, than those for the isolated particles, and the height distribution is very inhomogeneous. Note that the spatial scale for the local field distribution is much larger than the metal grain size a_0 chosen to be unity for all the figures. Therefore the main assumption of effective medium theory^{13,38-43} that the local fields are the same for all metal grains fails for the frequencies of the plasmon resonance and nonvanishing concentrations p . We emphasize a strong resemblance in the field distributions for p and $1 - p$ [cf. Figs. 2(a) and 2(g), 2(b) and 2(f), 2(c) and 2(e)].

For larger wavelengths, a single metal grain is off the plasmon resonance. Nevertheless, as one can see from Figs. 3(a)–3(d), the local field fluctuations are even larger than those at the plasmon resonance frequency. At these wavelengths, clusters of the conducting particles (rather than individual particles) resonate with the external field oscillations. Therefore, it is not surprising that the local field distributions are quite different from those in Fig. 2. In Fig. 3, we show the field distributions at the percolation threshold $p = p_c = 0.5$ for different wavelengths, namely, Fig. 3(a): $\lambda = 0.5$ μm , Fig. 3(b): $\lambda = 1.5$ μm , Fig. 3(c): $\lambda = 10$ μm , and Fig. 3(d): $\lambda = 20$ μm . Note that the field intensities in peaks increase with λ , reaching very high values $\sim 10^5 |E^{(0)}|^2$; the peak spatial separations increase with λ as well. These results are also in contradiction with effective medium theory that predicts strong field fluctuations³⁰ in the vicinity of plasmon resonance frequency ω_r only. In the next section, we present a scaling theory for the field distributions on a semicontinuous film that explains the above results of the simulations.

The field pattern obtained in our simulations resembles the experimentally measured field distribution in percolating metal-dielectric films in the microwave band.³⁵ We note that we simulate films in such a way that samples with the same p correspond to identical films. Thus from Fig. 4, we can conclude that spatial locations of the field peaks strongly

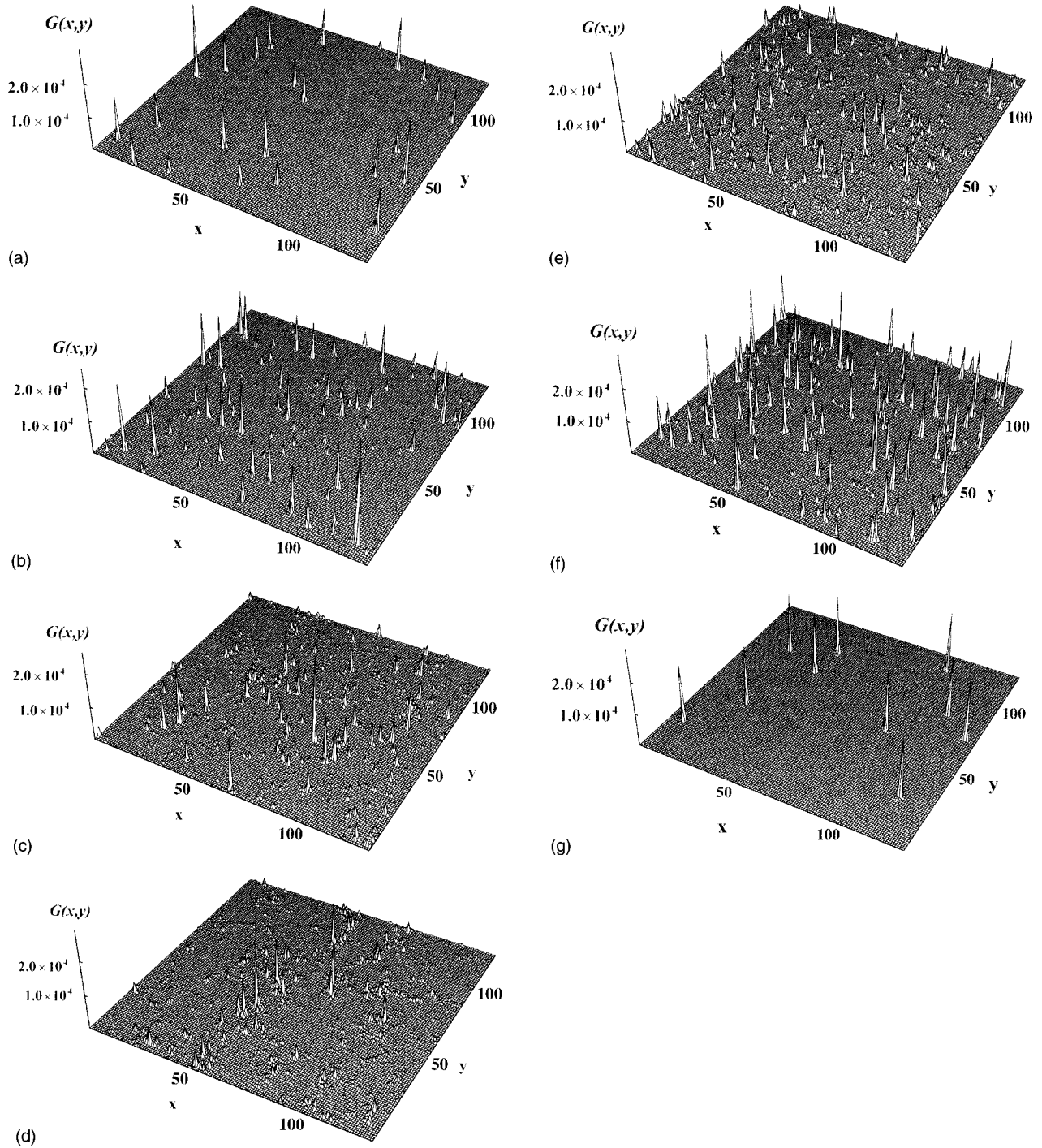


FIG. 2. Distribution of the local field intensities $G(x,y)=|E(x,y)|^2/|E^{(0)}|^2$ on a metal (silver) semicontinuous film for $\epsilon'_m = -\epsilon_d = -2.2$ ($\lambda \approx 365$ nm) at different metal concentrations p . (a) $p=0.001$, (b) $p=0.01$, (c) $p=0.1$, (d) $p=0.5$, (e) $p=0.9$, (f) $p=0.99$, and (g) $p=0.999$.

depend on frequency. Qualitatively similar results were previously demonstrated for fractals and self-affine films in the optical spectral range.^{21,24} Thus by changing the frequency one can excite different nm-size hot spots on the film. This effect is of great importance for various applications, and it can be studied experimentally in the optical spectral range using near-field scanning optical microscopy providing sub-wavelength resolution.^{23,58,63} In the microwave range it can be studied easily by the local probe method developed recently.³⁵ We note that there are nontrivial correlations in

the positions of different peaks;³³ they are not necessarily associated with different clusters independently resonating with the applied field. For instance, some peaks that one might think of as different modes, in reality, are spatially disconnected parts of the same mode; in other cases, however, different peaks do correspond to different modes.

We emphasize that all results are shown in natural linear scales. What we see in Figs. 2 and 3 is the top part of the field distribution, i.e., the largest fields only. The fields in other points forming a background, although smaller, are not,

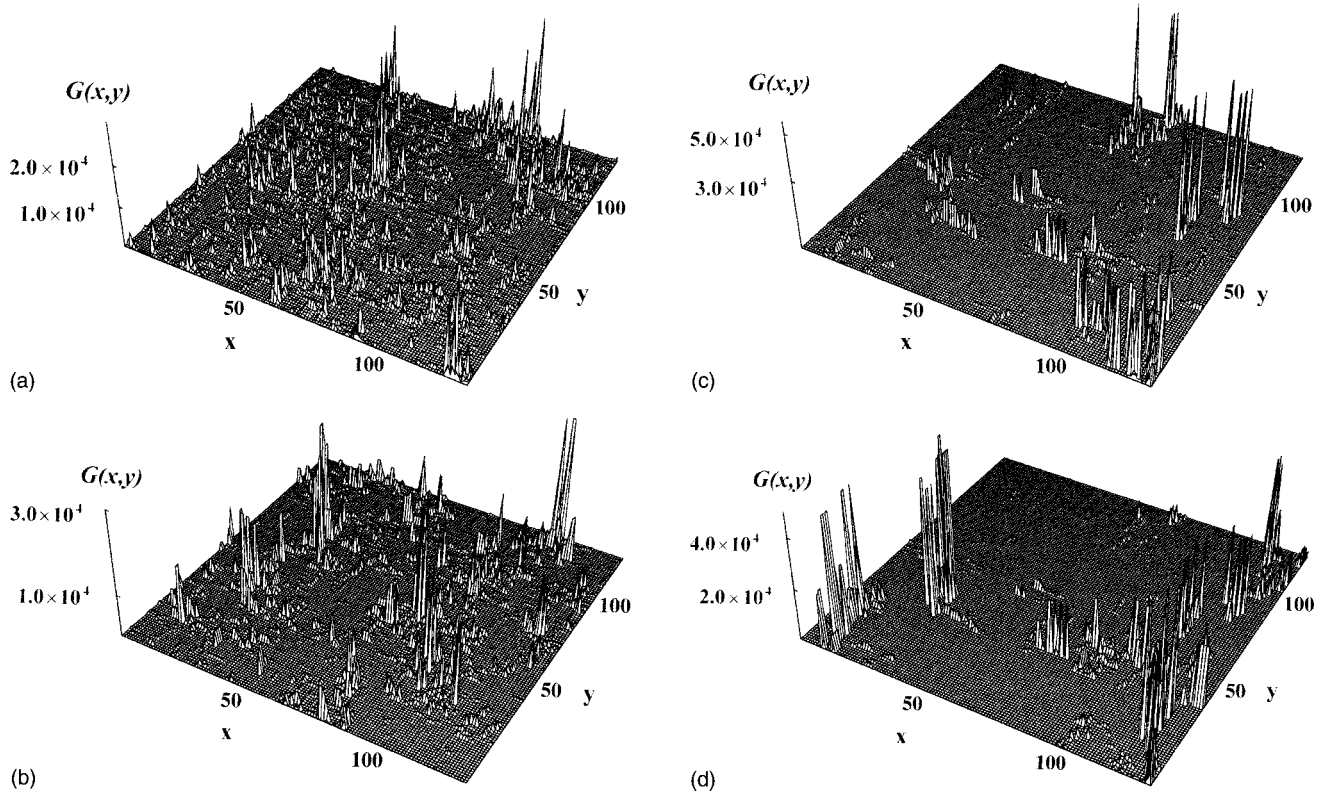


FIG. 3. Distribution of the local field intensities $G(x,y)=|E(x,y)|^2/|E^{(0)}|^2$ in a semicontinuous film at the percolation threshold for different wavelengths. (a) $\lambda=0.5 \mu\text{m}$, (b) $\lambda=1.5 \mu\text{m}$, (c) $\lambda=10 \mu\text{m}$, and (d) $\lambda=20 \mu\text{m}$.

of course, zero. However, for the nonlinear optical effects studied here the largest fields play the most important roles and the smaller background fields (that are not seen in the figures) can be neglected in most cases.

In Fig. 4, we also show results of our calculations for the average enhancements for the intensity of the local fields $\langle |\mathbf{E}(\mathbf{r})|^2 \rangle / |\mathbf{E}^{(0)}|^2$. The results are presented as a function of p

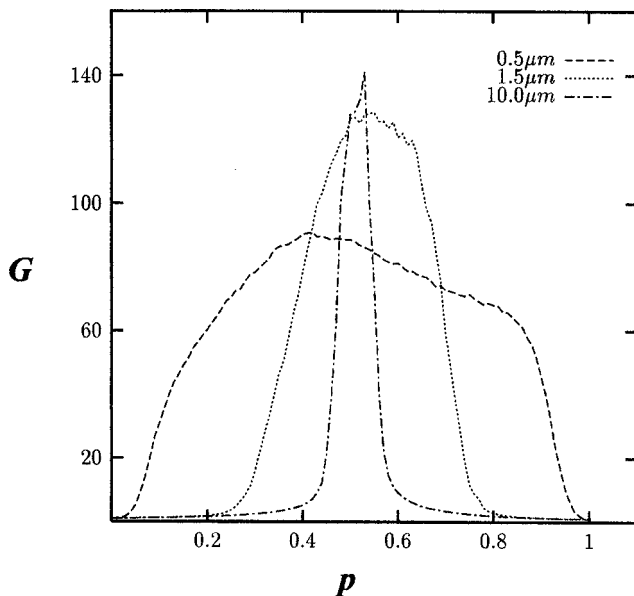


FIG. 4. The average enhancement of the field intensity $G = \langle |\mathbf{E}(\mathbf{r})|^2 \rangle / |\mathbf{E}^{(0)}|^2$ on a silver semicontinuous film as a function of the metal concentration p for three different wavelengths.

for different wavelengths $\lambda=0.5 \mu\text{m}$, $\lambda=1.5 \mu\text{m}$, and $\lambda=10 \mu\text{m}$. We see that the field enhancements are large, on average, ($\sim 10^2$) but much smaller than in the local peaks in Fig. 3. This is because the largest peaks are separated by relatively large distances so that the average enhancement is not as large as the local one in the peaks. The other moments of the field distribution, which are important for an estimation of the nonlinear response, experience even stronger enhancement, especially for concentrations close to the percolation threshold. For example, the fourth moment $\langle |\mathbf{E}(\mathbf{r})|^4 \rangle / |\mathbf{E}^{(0)}|^4$ exceeds the value 10^6 for $p=p_c$ and $\lambda > 1 \mu\text{m}$. This is not surprising since the local fields raised to the fourth power, $|\mathbf{E}(\mathbf{r})|^4 / |\mathbf{E}^{(0)}|^4$, reach in the peaks the values 10^{10} , as follows from Fig. 3.

The range of p , where the enhancements occur is very large in the visible range ($\Delta p = |p - p_c| \approx 0.45$). However, it shrinks towards larger wavelengths, as seen in the figure. From the above results, it follows that the local fields experience strong space fluctuations on a semicontinuous film; the large fields in the peaks result in giant enhancements of the optical nonlinearities considered below.

III. SCALING THEORY OF THE FIELD FLUCTUATIONS AND THE HIGH-ORDER FIELD MOMENTS

As pointed out above the spatial field fluctuations on a semicontinuous metal film have the form of huge local fields within spatially separated peaks on the film. One could anticipate that the local fields are strong on a semicontinuous film for ω slightly smaller than ω_p^* —the renormalized plasma frequency introduced above by Eq. (2). For the fre-

quency range $\omega \ll \omega_p^*$, the real part of the metal dielectric constant ε_m is negative and its absolute values are of the order of unity, i.e., they are close to the dielectric constant of the film substrate ε_d . Therefore, the conductivities of the L - R and C elements in the equivalent network have opposite signs and they are close to each other in absolute values. [The exact resonance condition occurs in our model at $\omega = \omega_r < \omega_p^*$, which corresponds to the requirement $\text{Re}(\varepsilon_m) = -\varepsilon_d$.] Thus, a semicontinuous film can be thought of as a system of contours tuned in resonance with the frequency of the external field. These resonance modes are seen as giant spatial fluctuations in the field distributions over the film. In the dilute case $p \ll 1$ these resonances are associated with plasmon resonances of individual metal grains.

What might be more surprising is the fact that the giant fluctuations of the local fields also occur for $\omega \ll \omega_p^*$, when the contrast $H = |\varepsilon_m|/\varepsilon_d \gg 1$. If the contrast $H \gg 1$, the conductivity of the L - R and C elements of the equivalent network are quite different and a single contour cannot be excited by the external field. However, as our numerical simulations show, the field fluctuations become larger with the increase of the wavelength λ toward the infrared spectral range (see Fig. 3).

To understand the origin of the giant field fluctuations for the large contrast $H \gg 1$, we invoke scaling arguments of percolation theory.⁴⁶ Below we develop further the scaling approach from our previous works^{33,34} and apply it for calculating the high-order field moments.

Since enhancements for the nonlinear optical processes have maxima near the percolation threshold p_c , we assume first that the concentration of the conducting particles p is exactly equal to the percolation threshold $p = p_c$. We consider the case when the frequency ω is much smaller than the plasma frequency $\omega \ll \omega_p$, so that the contrast is large and can be approximated as $H \approx (\omega_p/\omega)^2/\varepsilon_d \gg 1$ for a Drude metal. We also assume that $\omega \gg \omega_\tau$, i.e., losses in metal grains are relatively small.

To find the field distributions over the system, we apply the renormalization procedure first suggested in Refs. 67,68. We divide a system into squares of size l and consider each square as a new element. All such squares can be classified into two types. A square that contains a path of conducting particles spanning over is considered as a ‘‘conducting’’ element. A square without such an ‘‘infinite’’ cluster is considered as a nonconducting dielectric element. Following finite size arguments,^{17,46,67,68} the effective dielectric constant of the conducting square $\varepsilon_m^*(l)$ decreases with increasing size l as

$$\varepsilon_m^*(l) \cong (l/a_0)^{-t/\nu_p} \varepsilon_m, \quad (21)$$

where a_0 is the average size of metal grains and t and ν_p are the critical exponents for the conductivity and the percolation correlation length, respectively. For a 2D system $t \approx \nu_p = 4/3$.^{12,17,46} The effective dielectric constant of a dielectric square $\varepsilon_d^*(l)$ increases with increasing size l as

$$\varepsilon_d^*(l) \cong (l/a_0)^{s/\nu_p} \varepsilon_d, \quad (22)$$

where s is the critical exponent for the static dielectric constant; $s \approx \nu_p = 4/3$, for a 2D system.^{12,17,46} We now set the square size l to be equal to l^* :

$$l = l^* = a_0 (|\varepsilon_m'|/\varepsilon_d)^{\nu_p/(t+s)}, \quad (23)$$

where $\varepsilon_m' + i\varepsilon_m'' \equiv \text{Re}(\varepsilon_m) + i\text{Im}(\varepsilon_m)$. Then, in the renormalized system, where each square of size l^* is considered as a single element, the ratio of the dielectric constants of these new elements is equal to

$$\varepsilon_m^*(l^*)/\varepsilon_d^*(l^*) \cong \varepsilon_m/|\varepsilon_m'| = -1 + i\kappa, \quad (24)$$

where the loss factor $\kappa = \varepsilon_m''/|\varepsilon_m'| \approx \omega_\tau/\omega \ll 1$. (Recall that in the visible and infrared spectral ranges the real part of the metal dielectric constant ε_m' is negative and large in magnitude, $|\varepsilon_m'| \gg \varepsilon_d$.)

It follows from Eq. (24) that the renormalized system is a system of the L - R and C elements tuned in the resonance. Therefore, the local electric fields $\mathbf{E}^*(\mathbf{r})$ are significantly enhanced in comparison with the macroscopic field $\mathbf{E}^{(0)}$. As shown in Ref. 33, in a 2D system with the ratio of ε_m^* to ε_d^* given by Eq. (24), the field E^* can be estimated as

$$E^* \cong \sqrt{\langle |\mathbf{E}^*(\mathbf{r})|^2 \rangle} \cong E^{(0)} \kappa^{-\gamma/2} \gg E^{(0)}, \quad (25)$$

where the critical exponent γ introduced in Ref. 33 is near unity, $\gamma \approx 1.0$.

In the renormalized system the local field $\mathbf{E}^*(\mathbf{r})$ is still strongly inhomogeneous. Really, we see the spatially separated peaks in Fig. 2 where the field distributions are shown for the frequency $\omega = \omega_r$ corresponding to the plasmon resonance in a metal grain, i.e., for $\text{Re}[\varepsilon_m(\omega)] = -\varepsilon_d$ [cf. Eq. (24)]. The spatial scale ξ_e^* for the field fluctuations in the renormalized (resonance) system have been estimated in Refs. 32,33 as

$$\xi_e^* \propto \kappa^{-\nu_e}, \quad (26)$$

where the critical exponent is equal to $\nu_e = 0.4 - 0.5$. Therefore, the field distribution in the renormalized system might be thought of as a set of peaks with amplitude

$$E_m^* \cong E^*(\xi_e^*/a_0) \quad (27)$$

separated by distance ξ_e^* so that $E^{*2} \cong \langle |\mathbf{E}^*(\mathbf{r})|^2 \rangle \cong E_m^{*2}/(\xi_e^*/a_0)^2$.

Now we can estimate the field fluctuations in the original system. A typical configuration of conducting clusters that resonate at frequency $\omega \ll \omega_p$ is sketched in Fig. 5. The gap between the two conducting clusters A and B has a capacity conductance $\Sigma_c^{AB}(l) \approx -i\omega\varepsilon_d^*(l)a_0/4\pi$ that depends on the size l of the considered clusters. The conducting paths coming to the gap have an inductive conductance Σ_i^{AB} ; this is because the metal conductivity is inductive for $\omega < \omega_p^*$ ($\varepsilon_m' < 0$, $|\varepsilon_m'| \gg \varepsilon_m''$). The effective value of Σ_i^{AB} can be estimated from a simple observation that a conducting square of the size l has a typical conductivity $-i\omega\varepsilon_m^*(l)/4\pi$ that we attribute to the presence of the conducting path. Thus, we obtain $\Sigma_i^{AB}(l) \approx -i\omega\varepsilon_m^*(l)a_0/4\pi$. We chose the size $l = l^*$ so that capacitive and inductive conductances are equal to each other in modulus, $|\Sigma_c^{AB}(l^*)| \approx |\Sigma_i^{AB}(l^*)|$. Then there is a resonance in the configuration presented in Fig. 5. Note that

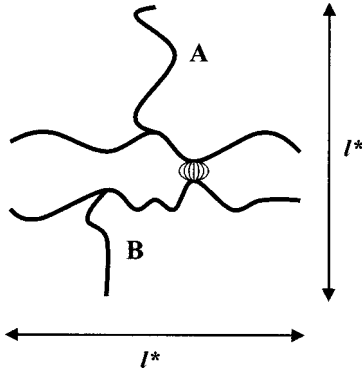


FIG. 5. Typical configuration of the conducting clusters that resonate at the frequency ω smaller than renormalized plasma frequency ω_p^* .

intercluster capacity conductance $\Sigma_c^{AB}(l)$ increases with cluster size l , whereas inductive conductance $\Sigma_i^{AB}(l)$ decreases with increasing l . Therefore, we can always find proper pairs of clusters with the size $l=l^*$ to fulfill the resonance condition $|\Sigma_c^{AB}(l^*)|=|\Sigma_i^{AB}(l^*)|$ for any large (in modulus) value of the metal dielectric constant $\varepsilon_m(\omega)$ provided $\varepsilon_m'(\omega) < 0$ (i.e., $\omega < \omega_p^*$).

Since the resonance clusters interact with each other, the local field concentrates in some subset of them only. The average distance between the field maximums in the renormalized system is equal to ξ_e^* [see Eq. (26)] and the average distance ξ_e between the field maximums in the original system can be estimated as

$$\xi_e \cong \xi_e^* l^* / a_0 \cong \kappa^{-\nu_e} l^* \cong a_0 (|\varepsilon_m' / \varepsilon_m''|)^{\nu_e} (|\varepsilon_m' / \varepsilon_d|)^{\nu_p / (t+s)} \quad (28)$$

which is much larger than the grain size $\xi_e \gg a_0$. This is the reason why the giant field fluctuations exist up to the far-infrared spectral range and their spatial structure is rather inhomogeneous as we can see in Figs. 3(a)–3(d).

In Fig. 5, we do not show the many finite conducting clusters that are always present in the system. These clusters are off resonance and, therefore, are not important for our consideration. Therefore, only a small part of the metal component is involved in the resonance excitation at any particular frequency of the applied field. Nevertheless, the resonance clusters cover almost the whole area of the film due to their fractal structure. Even for the resonance clusters, the local field is concentrated in only a small part of them. Accordingly, only a few metal grains actually carry most of the current. If we change the frequency, another set of metal clusters will resonate; these new resonating clusters still include only a small part of the metal.

The field E_{AB} in the intercluster gap is strongly enhanced for clusters with sizes $l=l^*$, yet the local field is strongly enhanced only for a part of these clusters as discussed above. We consider one such resonating cluster. The potential drop across the gap can be estimated as $U_{AB}^* \sim E_m^* l^*$ [see Eqs. (23) and (27)], and the local field is concentrated in the points of the close approach where the gap shrinks to a_0 . In the points of the close approach the local field acquires the largest values

$$E_m \cong E_m^* (l^* / a_0) \sim E^{(0)} (|\varepsilon_m' / \varepsilon_m''|)^{\gamma/2 + \nu_e} (|\varepsilon_m' / \varepsilon_d|)^{\nu_p / (t+s)}. \quad (29)$$

The points of the close approach determine the gap capacity conductance $\Sigma_c^{AB}(l^*)$ (cf. Ref. 7) that depends on the cluster size l^* . Therefore, the number $n_c(l^*)$ of the points of the close approach scales with size l^* in the same way as conductance Σ^{AB} ; namely, $n_c(l^*) \sim \Sigma^{AB}(l^*) \sim \varepsilon_d^*(l^*) \sim l^{*s/\nu_p}$ [see Eq. (22)].

The following pattern of the local field distribution emerges from these speculations: The largest local fields are concentrated in resonant clusters, in areas of the size l^* ; the areas with high local fields are separated in distance by the field correlation length $\xi_e \gg a_0$, given by Eq. (28). Within each resonant area there are $n_c(l^*)$ sharp peaks with amplitude $E_m(l^*)$. With an increasing wavelength of the incident wave (i.e., decreasing the frequency) the scale l^* increases, as do the amplitude E_m and the number of the local field maxima $n_c(l^*)$ in one resonating cluster; the average distance ξ_e between the resonant sets of the field peaks also increases with decreasing frequency. We can track this behavior of the field fluctuations in Fig. 3. For smallest frequencies [Figs. 3(c), 3(d)] the local fields have only a few groups of maxima. Typical distances between the groups of field peaks are much larger than a_0 (the grain size a_0 is chosen as unity in the figures). The number of peaks in each group increases systematically with decreasing frequency.

From this pattern of the local field distribution we obtain the following estimate for the moments of the local fields $\langle |\mathbf{E}(\mathbf{r})|^n \rangle$, in random semicontinuous metal films $\langle |\mathbf{E}(\mathbf{r})|^n \rangle \sim E_m^n n_c(l^*) / \xi_e^2$. The substitution in this equation of expressions of the field amplitude E_m [Eq. (29)], the field correlation length ξ_e [Eq. (28)], and the number of maxima in one cluster $n_c(l^*) \sim (l^*)^{s/\nu_p}$ gives

$$\langle |\mathbf{E}(\mathbf{r})|^n \rangle \cong |\mathbf{E}^{(0)}|^n (|\varepsilon_m' / \varepsilon_d|)^{n\nu_p / (t+s) - (2\nu_p - s) / (t+s)} \times (|\varepsilon_m' / \varepsilon_m''|)^{n(\gamma/2 + \nu_e) - 2\nu_e}. \quad (30)$$

For a 2D system, $t \approx s \approx \nu_p = 4/3$.^{12,17,46} Substituting these critical indices and $\gamma = 1$, $\nu_e = 0.5$ (Refs. 32,33) in Eq. (30) gives

$$\langle |\mathbf{E}(\mathbf{r})|^n \rangle \cong |\mathbf{E}^{(0)}|^n (|\varepsilon_m' / \varepsilon_d|)^{(n-1)/2} (|\varepsilon_m' / \varepsilon_m''|)^{n-1}. \quad (31)$$

Since in the visible, infrared, and far-infrared spectral ranges the real part of the dielectric constant of a typical metal is large, $|\varepsilon_m'| \gg \varepsilon_d$, whereas the losses are small, $\varepsilon_m'' \ll |\varepsilon_m'|$, the values of the field moments $\langle |\mathbf{E}|^n \rangle$ exceed the corresponding moments of the incident field $|\mathbf{E}^{(0)}|^n$ by several orders of magnitude. This indicates the presence of giant field fluctuations in semicontinuous metal films in the visible and, especially, in the infrared spectral ranges.

For the Drude metal, we can simplify Eq. (31) for sufficiently small frequencies, $\omega \ll \omega_p$, as

$$\langle |\mathbf{E}(\mathbf{r})|^n \rangle \cong |\mathbf{E}^{(0)}|^n \varepsilon_d^{(1-n)/2} \left(\frac{\omega_p}{\omega_\tau} \right)^{n-1}. \quad (32)$$

From this equation it follows that for frequencies $\omega \ll \omega_p$ the local field moments are independent of frequency.

Now we can estimate the local field moments for silver semicontinuous films [$\omega_p = 9.1$ eV, $\omega_\tau = 0.021$ eV (Ref. 71)].

Using $\varepsilon_d = 2.2$ typical for glass substrate, we obtain from Eq. (32) the estimate $\langle |\mathbf{E}|^n \rangle \approx 3 \times 10^2, 8 \times 10^4, 2.5 \times 10^7, 7 \times 10^9, \text{ and } 2 \times 10^{12}$ for $n = 2, 3, 4, 5, \text{ and } 6$, respectively, ($E^{(0)} = 1$).

The above estimates of the moments can be used, for example, for Raman scattering that does not depend on the phases of the local fields.^{34,36} Although Raman scattering is a linear process, its enhancement is proportional to $|\mathbf{E}|^4$ (Ref. 34) and in that sense is similar to nonlinear processes discussed in Ref. 21. From Eq. (32) we obtain the following expression for the enhancement G_{RS} of Raman scattering in semicontinuous metal films:

$$G_{\text{RS}} \sim \langle |\mathbf{E}(\mathbf{r})|^4 \rangle \sim \frac{|\varepsilon'_m|^{9/2}}{\varepsilon_d^{3/2} \varepsilon_m'^3}. \quad (33)$$

Note that this equation is somewhat different from that obtained in our previous work.³⁴ This difference is a consequence of the more detailed analysis of the local field fluctuations in the present paper. Nevertheless the main results of the rough scaling analysis³⁴ and the more elaborate consideration presented here are essentially the same: Surface enhancement of the Raman scattering on semicontinuous metal films is rather large, $G_{\text{RS}} \sim 10^5 - 10^7$, and independent of frequency for $\omega \ll \omega_p^*$ when the enhancement is proportional to $G_{\text{RS}} \sim (\omega_p / \omega_\tau)^3 / (\varepsilon_d)^{3/2}$.

Now we turn to nonlinear coherent processes. To estimate enhancements for nonlinear coherent processes, such as harmonic generation, one should average the nonlinear electric induction $D^{(n)} \propto \langle E^n \rangle$; the resultant enhancement is then given by $G^{(n)} \propto |D^{(n)}|^2 \propto \langle E^n \rangle^2$ (see, e.g., Ref. 21). Therefore, the parametric nonlinear optical processes are very sensitive to the relative phases of the fields at different points on the film. It is impossible to estimate enhancements, in general, considering only the absolute values of the field. However, we can estimate the upper limit for the enhancements assuming that all the fields are in phase. Formally, the upper limit for the enhancements can be obtained by neglecting the phase fluctuations, i.e., with the replacement of $\langle E^n \rangle$ for a nonlinear process of the n th order by $\langle |\mathbf{E}|^n \rangle$. By doing so, we obtain the estimate given by Eq. (31). We also note that the widely used ‘‘decoupling procedure’’ $\langle |\mathbf{E}|^n \rangle \rightarrow \langle |\mathbf{E}|^2 \rangle^{n/2}$ (see, for example, Refs. 13, 38, 42, 43) that works well in the static case,^{42,43} results in significantly underestimated (by several orders of magnitude) enhancement in the visible, infrared, and far-infrared spectral ranges, as follows from the above consideration. Accordingly, the mean-field theories based on the decoupling procedure are not applicable for an estimation of the optical nonlinearities in metal-dielectric composites with strong field fluctuations, which provide largest enhancements for various nonlinear effects.

It is instructive to summarize the above discussion and note that the field intensities in a random semicontinuous metal film $|\mathbf{E}(x, y)|^2$ can be viewed as groups of peaks with amplitudes $|\mathbf{E}_m| \gg |\mathbf{E}^{(0)}|$. Different groups of peaks are separated by distance $\xi_e \gg a_0$ [see Eqs. (28) and (29)]. The amplitudes of the peaks, as well as the typical distance between them, increases with decreasing frequency ω . This picture is in qualitative agreement with Figs. 3(a)–3(d), where the field fluctuations on a silver semicontinuous film are shown. We

would like to stress that despite the large distances between the peak groups, the field fluctuations can be highly correlated in space.³³

We should note that in the above estimations of the local field moments we implied that they do exist, i.e., we assumed that the moments converge when the size of a system increases. This is the case for incoherent processes (such as Raman scattering) which are phase insensitive and depend on the absolute values of the fields only, i.e., $\propto \langle |\mathbf{E}|^n \rangle$. However, as we show below, enhancements for coherent processes, which are proportional to $\langle E^n \rangle$ (rather than to $\langle |\mathbf{E}|^n \rangle$), do depend on the size of the system for sizes up to $L = 512$ used in our simulations. The reason for the size effect is probably the interference between the fields in different points of the film.

Above, for the sake of simplicity, we assumed that $p = p_c$. Now we estimate the concentration range $\Delta p = p - p_c$, where the above estimates for the local field moments are valid.^{33,34} Although the above estimates have been done for the percolation threshold $p = p_c$ they must also be valid in some vicinity to the threshold. Indeed the above speculations are based on the finite size scaling Eqs. (21) and (22), which hold until the scale l^* of the renormalized squares [see Eq. (23)] is smaller than the percolation correlation length $\xi_p \cong a_0(|p - p_c|/p_c)^{-\nu_p}$. At the percolation threshold, where the correlation length ξ_p diverges, our estimates are valid in a wide frequency range $\omega_\tau < \omega < \omega_p^*$ which includes the visible, infrared, and far-infrared spectral ranges for a typical metal. For any particular frequency from this interval, we estimate the concentration range Δp , where the giant field fluctuations occur, by equating the values of l^* from Eq. (23) and ξ_p . Thus we obtain the relation

$$|\Delta p| \leq (\varepsilon_d / |\varepsilon'_m|)^{1/(t+s)}. \quad (34)$$

For a 2D semicontinuous metal film, the critical exponents are $s \approx t \approx \nu_p = 4/3$, and the above relation acquires the form

$$|\Delta p| \leq (\varepsilon_d / |\varepsilon'_m|)^{3/8}. \quad (35)$$

For Drude metal, in the frequency range $\omega_p^* \ll \omega \ll \omega_\tau$, Eq. (35) can be rewritten as

$$\Delta p \leq \varepsilon_d^{3/8} (\omega / \omega_p)^{3/4}. \quad (36)$$

As follows from Eq. (36), the concentration range for the enhancement shrinks when the frequency decreases far below the renormalized plasma frequency ω_p^* [see Eq. (2)]. This result is in agreement with our computer simulations presented in Fig. 4.

It is important to note that although the above consideration of the local field distributions is based on the assumption of the large contrast $H \gg 1$, the estimation (36) reproduces the concentration interval for the giant field fluctuations for all the frequencies below ω_p^* (but larger than ω_τ) well. Also the estimate (33) *quantitatively* describes recent experimental studies of Raman scattering⁶⁰ in a semicontinuous metal film, as well as results of our computer simulations^{34,36} for the whole frequency range.

IV. GIANT ENHANCEMENTS OF OPTICAL NONLINEARITIES IN SEMICONTINUOUS METAL FILMS

In this section, we consider enhancements for different nonlinear optical processes on a semicontinuous metal film. Third- and second-order optical nonlinearities are analyzed. All numerical calculations are presented for $p = p_c$. The concentration region for the enhancement of nonlinearities was estimated in the previous section.

A. Kerr-type optical nonlinearities

The Kerr-type nonlinearities are third-order optical nonlinearities that result in addition to the linear electric induction \mathbf{D} a nonlinear term of the form

$$D_\alpha^{(3)}(\omega) = \varepsilon_{\alpha\beta\gamma\delta}^{(3)}(-\omega; \omega, \omega, -\omega) E_\beta E_\gamma E_\delta^*, \quad (37)$$

where

$$\varepsilon_{\alpha\beta\gamma\delta}^{(3)}(-\omega; \omega, \omega, -\omega) \quad (38)$$

is the third-order nonlinear dielectric constant,⁷² and \mathbf{E} is an electric field at frequency ω ; summation over repeated Greek indices is implied. The Kerr optical nonlinearity results in nonlinear corrections (proportional to the light intensity) for the refractive index and the absorption coefficient.

Below we consider macroscopically homogeneous and isotropic films and the normal incidence of light. Then the third-order terms in the average electric induction has in general the form

$$\langle \mathbf{D}^{(3)}(\mathbf{r}) \rangle = \alpha |\mathbf{E}^{(0)}|^2 \mathbf{E}^{(0)} + \beta E^{(0)2} \mathbf{E}^{(0)*}, \quad (39)$$

where $\mathbf{E}^{(0)}$ is the amplitude of the external (macroscopic) electric field at frequency ω , $E^{(0)2} \equiv (\mathbf{E}^{(0)} \cdot \mathbf{E}^{(0)})$, α and β are some constants [not to be confused with the tensor components in Eq. (37)]. Note that the second term in Eq. (39) for the nonlinear induction of an isotropic film can result in a change of the polarization of the incident light.⁷² Equation (39) simplifies for the case of linear and circular polarization of the incident light.⁷² For the linear polarization the complex vector $\mathbf{E}^{(0)}$ reduces to a real vector. Then the expressions $|\mathbf{E}^{(0)}|^2 \mathbf{E}^{(0)}$ and $E^{(0)2} \mathbf{E}^{(0)*}$ in Eq. (39) become the same and the equation can be rewritten as

$$\langle \mathbf{D}^{(3)}(\mathbf{r}) \rangle = \varepsilon_e^{(3)} |\mathbf{E}^{(0)}|^2 \mathbf{E}^{(0)}, \quad (40)$$

where the nonlinear dielectric constant $\varepsilon_e^{(3)}$ is scalar now. For the sake of simplicity, we consider below the linearly polarized incident wave. Equation (40) we rewrite in terms of the nonlinear average current $\langle \mathbf{j}^{(3)}(\mathbf{r}) \rangle$ and the effective Kerr conductivity $\sigma_e^{(3)} = -i\omega \varepsilon_e^{(3)}/4\pi$; this gives

$$\langle \mathbf{j}^{(3)}(\mathbf{r}) \rangle = \sigma_e^{(3)} |\mathbf{E}^{(0)}|^2 \mathbf{E}^{(0)}. \quad (41)$$

This form of Kerr nonlinearity is used in the discussion below.

Consider the case when the nonlinearities in metal grains of a semicontinuous film and dielectric substrate are negligible, and the film is covered by molecules possessing the Kerr-type nonlinearity. We still assume that the film is thin enough to consider the local electric field as homogeneous in

a direction perpendicular to the film plane. Then the current in a semicontinuous film with the adsorbed nonlinear molecules on it is equal to

$$\mathbf{j}(\mathbf{r}) = \sigma(\mathbf{r}) \mathbf{E}'(\mathbf{r}) + \sigma^{(1)}(\mathbf{r}) \mathbf{E}'(\mathbf{r}) + \sigma^{(3)}(\mathbf{r}) |\mathbf{E}'(\mathbf{r})|^2 \mathbf{E}'(\mathbf{r}), \quad (42)$$

where $\mathbf{E}'(\mathbf{r})$ is the local fluctuating field at the coordinate \mathbf{r} of the film, $\sigma(\mathbf{r})$ is the local film conductivity, and $\sigma^{(1)}(\mathbf{r})$ and $\sigma^{(3)}(\mathbf{r})$ are the linear and Kerr-type nonlinear conductivities of the adsorbed molecular layer. By using this expression in the current conservation law given by Eq. (5) we obtain [cf. Eq. (16)]

$$\nabla \left([\sigma(\mathbf{r}) + \sigma^{(1)}(\mathbf{r})] \left[-\nabla \phi(\mathbf{r}) + \mathbf{E}^{(0)} + \frac{\sigma^{(3)}(\mathbf{r})}{\sigma(\mathbf{r}) + \sigma^{(1)}(\mathbf{r})} \mathbf{E}'(\mathbf{r}) |\mathbf{E}'(\mathbf{r})|^2 \right] \right) = 0, \quad (43)$$

where $\mathbf{E}^{(0)}$ is the applied electric field, and $-\nabla \phi(\mathbf{r}) + \mathbf{E}^{(0)} = \mathbf{E}'(\mathbf{r})$ is the local field. By considering the last term in the square brackets as an external inhomogeneous field we obtain from Eq. (15) the equation for the average current

$$\langle \mathbf{j}(\mathbf{r}) \rangle = \mathbf{E}^{(0)} \left[\sigma_e^{(0)} + \frac{\langle \sigma^{(3)}(\mathbf{r}) [\mathbf{E}(\mathbf{r}) \cdot \mathbf{E}'(\mathbf{r})] |\mathbf{E}'(\mathbf{r})|^2 \rangle}{E^{(0)2}} \right], \quad (44)$$

where $\sigma_e^{(0)}$ and $\mathbf{E}(\mathbf{r})$ are the effective conductivity and local fluctuating field, respectively, obtained in the linear approximation, i.e., for $\sigma^{(3)} \equiv 0$. Comparing Eqs. (44) and (41), we find the equation for the effective Kerr conductivity

$$\sigma_e^{(3)} = \frac{\langle \sigma^{(3)}(\mathbf{r}) [\mathbf{E}(\mathbf{r}) \cdot \mathbf{E}'(\mathbf{r})] |\mathbf{E}'(\mathbf{r})|^2 \rangle}{E^{(0)2} |\mathbf{E}^{(0)}|^2}. \quad (45)$$

In this paper, we consider the case of weak nonlinearities. Then the local field $\mathbf{E}'(\mathbf{r})$ in Eq. (45) can be replaced by the linear local field $\mathbf{E}(\mathbf{r})$ resulting in the following equation for the Kerr conductivity:

$$\sigma_e^{(3)} = \frac{\langle \sigma^{(3)}(\mathbf{r}) E^2(\mathbf{r}) |\mathbf{E}(\mathbf{r})|^2 \rangle}{E^{(0)2} |\mathbf{E}^{(0)}|^2}, \quad (46)$$

which reproduces the formula (20).

Now we suppose for simplicity that the Kerr-type nonlinear surface conductivities of the adsorbed molecules $\sigma^{(3)}$ are uniformly distributed over the film surface. Then Eq. (46) simplifies to

$$\sigma_e^{(3)} = \sigma^{(3)} \frac{\langle E^2(\mathbf{r}) |\mathbf{E}(\mathbf{r})|^2 \rangle}{E^{(0)2} |\mathbf{E}^{(0)}|^2}. \quad (47)$$

In the absence of metal grains the effective nonlinear Kerr conductivity $\sigma_e^{(3)}$ coincides with the Kerr conductivity $\sigma^{(3)}$ of the layer of the adsorbed nonlinear molecules. Therefore the enhancement of the Kerr nonlinearity G_K is given by the equation

$$G_K = \frac{\langle E^2(\mathbf{r})|\mathbf{E}(\mathbf{r})|^2 \rangle}{E^{(0)2}|\mathbf{E}^{(0)}|^2}. \quad (48)$$

From the above equation it follows that the enhancement of the Kerr nonlinearity is expressed in terms of the local field $\mathbf{E}(\mathbf{r})$ found in the linear approximation; this field experiences the giant fluctuations studied in Secs. II and III.

Above we assumed that the nonlinear Kerr conductivity $\sigma^{(3)}$ is due to the adsorbed molecules covering the film. In some cases, the nonlinear response can also be due to the metal and/or dielectric grains forming the film, with no adsorbed molecules on it. If this is the case, $\sigma^{(3)}(\mathbf{r})$ in Eq. (42) is the nonlinear conductivity of the grain, and the sum of the linear conductivities $\sigma(\mathbf{r}) + \sigma^{(1)}(\mathbf{r})$ of the grain and adsorbed molecule should be replaced in Eq. (42) by the linear conductivity of the grain itself $\sigma(\mathbf{r})$. Repeating the above derivations after the Eq. (42), we arrive at the following result for the effective Kerr conductivity:

$$\sigma_e^{(3)} = p\sigma_m^{(3)} \frac{\langle E^2(\mathbf{r})|\mathbf{E}(\mathbf{r})|^2 \rangle_m}{E^{(0)2}|\mathbf{E}^{(0)}|^2} + (1-p)\sigma_d^{(3)} \frac{\langle E^2(\mathbf{r})|\mathbf{E}(\mathbf{r})|^2 \rangle_d}{E^{(0)2}|\mathbf{E}^{(0)}|^2}, \quad (49)$$

where $\langle \dots \rangle_m$ and $\langle \dots \rangle_d$ stand for the averaging over the metal and dielectric grains, respectively, and $\sigma_m^{(3)}$ and $\sigma_d^{(3)}$ are the corresponding nonlinear conductivities. Formula (49) for enhancement of the cubic nonlinearity in percolating composites was previously obtained by Aharony,⁸ Stroud and Hui,⁹ and Bergman.¹¹ A similar formula was independently obtained by Shalaev *et al.* to describe the Kerr enhancement in aggregates of metal particles.¹⁹⁻²¹

Note that $\mathbf{E}^{(0)}$ in Eqs. (6) and (43) is actually the average macroscopic field that can be, in general, different from the incident field \mathbf{E}_{inc} . For the thin 2D films considered here in the quasistatic limit, the macroscopic field is constant and related to the incident field through the transmittance T as $\mathbf{E}^{(0)} = T\mathbf{E}_{\text{inc}}$ (see discussion in Ref. 34). Above we defined the enhancement factor as the ratio of nonlinear signals from a film with and without metal grains on it. This means that in the denominator of expression (48) we should replace $|\mathbf{E}^{(0)}|^4$ by $|\mathbf{E}_{\text{inc}}|^4 = |\mathbf{E}^{(0)}|^4/T^4$; this gives an additional prefactor T^4 in formula (48), if by $\mathbf{E}^{(0)}$ we mean the macroscopic field. (For a purely dielectric film without metal grains, we can set $T_d = 1$ and $\mathbf{E}^{(0)} = \mathbf{E}_{\text{inc}}$.) For the sake of simplicity, hereafter we omit this prefactor associated with the transmittance T . To take it into account one should do the above replacement $\mathbf{E}^{(0)} \rightarrow \mathbf{E}^{(0)}/T$ in the denominators of the following formulas for the enhancements of nonlinear optical processes.

According to Eq. (48) the value of the Kerr enhancement G_K is proportional to the fourth power of the local field averaged over the sample. This is similar to the case of surface-enhanced Raman scattering having the enhancement factor^{34,36}

$$G_{\text{RS}} = \frac{\langle |\sigma(\mathbf{r})|^2 |\mathbf{E}(\mathbf{r})|^4 \rangle}{|\sigma_d|^2 |\mathbf{E}^{(0)}|^4}. \quad (50)$$

(Note that in Refs. 34,36 a different notation, A , was used for G_{RS} .) We note, however, that G_K is complex, whereas G_{RS} is a real positive quantity. Because the enhancement for Ra-

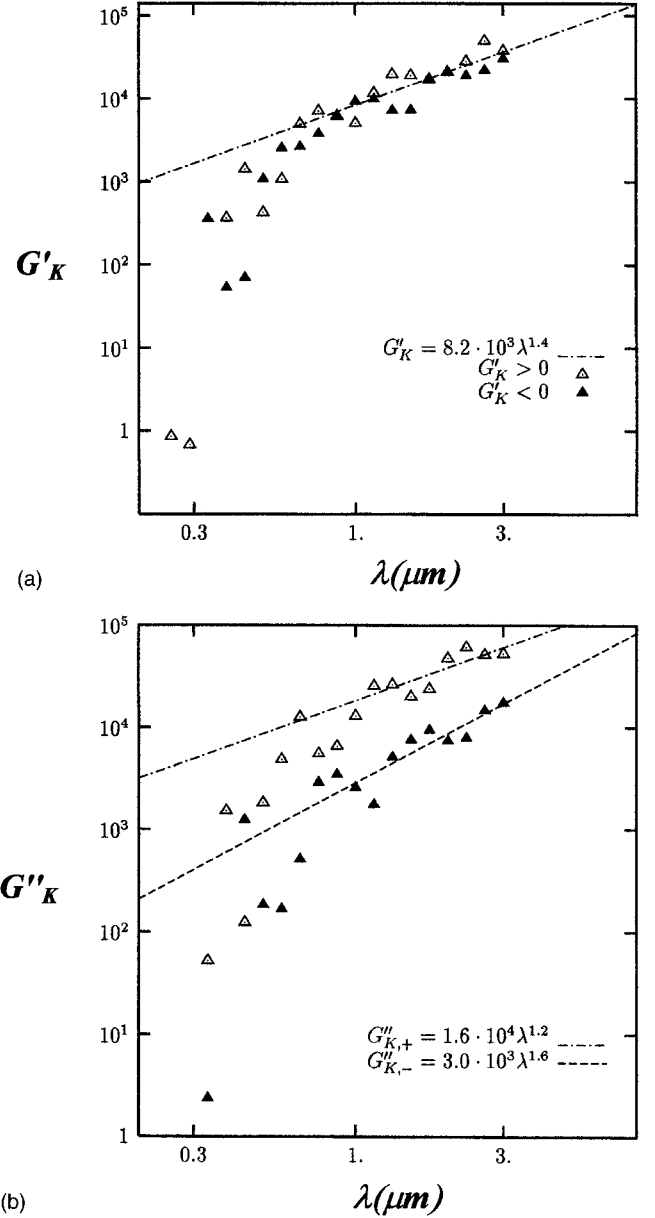


FIG. 6. The average Kerr-nonlinearity enhancements (real G'_K and imaginary G''_K parts) on a silver semicontinuous film as a function of wavelengths (a): G'_K , (b): G''_K . In all cases, $p = p_c$. The open triangles correspond to the positive values $G'_K > 0$ and $G''_K > 0$; the solid triangles stand for the negative values $G'_K < 0$ and $G''_K < 0$. The film sizes are 512×512 .

man scattering is determined by the average of $|\mathbf{E}|^4$, which is phase insensitive, the upper limit for the enhancement is realized in this case [see Eq. (33) and the accompanying discussion]. In accordance with this, our results of numerical simulations^{34,36} are well described by the scaling formula (33).

Below we present results of our numerical simulations for the surface-enhanced Kerr-nonlinearity in a semicontinuous metal film at the percolation threshold. We used formula (48) for calculating the enhancement; the local fields were found following the numerical procedure described in the previous section. We generated an ensemble of 100 random films with the size 512×512 . In Figs. 6 we show the average enhancements for the real and imaginary parts of the Kerr-

nonlinearity enhancement, G'_K and G''_K , as functions of the wavelength (the data are given for silver films). Note that for both quantities G'_K and G''_K not only the magnitude but also the sign depends strongly on the wavelength. (The positive values are given by open triangles, the solid triangles represent the negative values.) For G'_K , the positive and negative values are close in magnitudes and their dependence on the wavelength λ can be roughly approximated as $|G'_K| \sim \lambda^{q_1}$, where the exponent $q_1 = 1.4 \pm 0.2$. For G''_K , the magnitudes of the positive values are systematically larger than those for the negative values; the wavelength dependence of the positive enhancements $G''_K > 0$ is approximated as $G''_K > 0 \sim \lambda^{q_2}$, $q_2 = 1.2 \pm 0.3$, and the dependence of the negative enhancements is approximated as $G''_K < 0 \sim \lambda^{q_3}$, $q_3 = 1.6 \pm 0.3$. The strong enhancement of the Kerr nonlinearity toward the long wavelength part of the spectrum is due to the increase of the local fields in this part of the spectrum (see Figs. 3).

The real and imaginary parts of G_K are responsible for the enhancement of the nonlinear refractive index and absorption, respectively. The above calculations were performed, however, in the quasistatic approximation which does not account for wave propagation effects. Still, the above results can be used for a description of samples that are large compared to the wavelength. For example, they can be applied for a large (in comparison with λ) multilayer system composed of many subwavelength-size films such as the ones considered above; then, the obtained formulas define the enhanced microscopic nonlinear responses for each layer of the multilayer system.

According to the above calculations, the enhancement is very large and reaches, on average, values $\sim 10^4$ at $\lambda \sim 1 \mu\text{m}$ (the enhancement further increases for larger wavelengths). Such strong enhancements for the Kerr nonlinearities in semicontinuous metal films indicate their high potential for various applications based on large $\sigma_e^{(3)}$ (or $\varepsilon_e^{(3)}$); for example, optical switches. A semicontinuous metal film might also be used as a Fresnel lens in different applications.

B. Four-wave mixing

So far we considered optical responses of a semicontinuous metal film to a single incident light beam. A number of nonlinear optical processes occur when several beams with, in general, different frequencies are incident on a film. In this paper, we consider four-wave mixing (FWM) as a typical process of this kind. The FWM is determined by a nonlinear electric induction similar to Eq. (37);⁷²

$$D_\alpha^{(3)}(\omega) = \varepsilon_{\alpha\beta\gamma\delta}^{(3)}(-\omega_s; \omega_1, \omega_1, -\omega_2) E_\beta^{(1)} E_\gamma'^{(1)} E_\delta^{*(2)}, \quad (51)$$

where $\omega_s = 2\omega_1 - \omega_2$ is the frequency of a field that is generated as a result of the wave mixing, ω_1 is the frequency of the incident waves with the amplitudes $\mathbf{E}^{(1)}$ and $\mathbf{E}'^{(1)}$, and ω_2 is the frequency of the incident wave with the amplitude $\mathbf{E}^{(2)}$. Note that the induction in Eq. (51) is proportional to the complex conjugate of the applied field $\mathbf{E}^{(2)}$ which indicates that the generated wave can be thought of as a time-reversed $\mathbf{E}^{(2)}$ wave; this effect of the optical phase conjugation (OPC) makes possible the restoring of the wave phase-front.⁷²

Coherent anti-Stokes Raman scattering is an example of the FWM. In one elementary act of the coherent anti-Stokes Raman process, the two ω_1 photons are converted into one ω_2 and one ω_s photon. Another example is degenerate FWM; this process is used for the above mentioned optical phase conjugation that can result in the complete removal of optical aberrations.⁷² In degenerate FWM, all waves have the same frequency ($\omega_s = \omega_1 = \omega_2$) and differ only in their propagation directions and, in general, in their polarizations. In a typical OPC experiment, two oppositely directed pump beams, with field amplitudes $\mathbf{E}^{(1)}$ and $\mathbf{E}'^{(1)}$, and a probe beam, with amplitude $\mathbf{E}^{(2)}$ (directed at some small angle with respect to the pump beams), result in the OPC beam that propagates against the probe beam, i.e., the wave vector \mathbf{k}_s of the new OPC beam generated in the FWM process is equal to $\mathbf{k}_s = -\mathbf{k}_2$.

Because of the interaction geometry, the wave vectors of the beams satisfy the relation $\mathbf{k}_1 + \mathbf{k}_1' = \mathbf{k}_2 + \mathbf{k}_s = 0$. Clearly, for the two pairs of oppositely directed beams with the same frequency ω the phase-matching conditions are automatically fulfilled making the OPC possible.⁷²

For simplicity, we consider the degenerated FWM (DFWM) process where all the components of the total applied field $\mathbf{E}^{(0)} = \mathbf{E}^{(1)} + \mathbf{E}'^{(1)} + \mathbf{E}^{(2)}$ have the same amplitude and polarizations. The effective nonlinear conductivity (dielectric constant) $\sigma_e^{(3)}$ ($\varepsilon_e^{(3)} = i4\pi\sigma_e^{(3)}/\omega$), which results in the DFWM, coincides with the above considered nonlinear conductivity, which is responsible for the Kerr optical nonlinearity. Note also that the above nonlinear conductivity $\sigma_e^{(3)}$ can be associated with either the metal-dielectric film itself or molecules adsorbed on it. We first assume the latter to be the case.

For coherent effects, including the ones discussed in this section, the averaging is performed for the generated field amplitude (rather than intensity) or, equally, for the nonlinear current in the system.^{21,34} As shown in the previous section, the average nonlinear electric current, with the nonlinear conductivity given by Eq. (41) is $\mathbf{j}^{(3)}(\omega) \propto \sigma_e^{(3)} = \sigma^{(3)} G_K$. The signal for coherent processes is proportional to $|\mathbf{j}^{(3)}|^2 \propto |\sigma_e^{(3)}|^2$. Thus we conclude that the resultant enhancement for the degenerate (or nearly degenerate) in frequency four-wave mixing can be expressed in terms of the enhancement for the Kerr conductivity as

$$G_{\text{FWM}} = \left| \frac{\sigma_e^{(3)}}{\sigma^{(3)}} \right|^2 = |G_K|^2 = \frac{|\langle E^2(\mathbf{r}) |\mathbf{E}(\mathbf{r})|^2 \rangle|^2}{|E^{(0)}|^8}. \quad (52)$$

If the nonlinear conductivity $\sigma^{(3)}$ is due to metallic grains in the film (rather than due to the adsorbed nonlinear molecules), the formula (52) should be replaced by

$$G_{\text{FWM}} = p^2 \frac{|\langle E^2(\mathbf{r}) |\mathbf{E}(\mathbf{r})|^2 \rangle|^2}{|E^{(0)}|^8}. \quad (53)$$

[See also Eq. (49).]

The numerical calculations for FWM were performed as above for 100 random samples of the 512×512 size each. In Figs. 7 we show the average enhancement G_{FWM} as a function of the wavelength at $p = p_c$. The calculations were performed based on formula (52). Similar to the Kerr effect, the

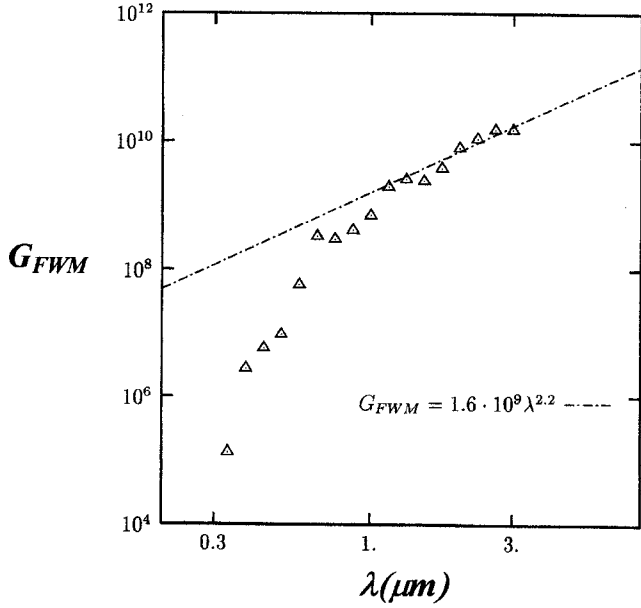


FIG. 7. The average FWM enhancement G_{FWM} on a silver semi-continuous film as a function of the wavelength at $p=p_c$. The film sizes are 512×512 .

average enhancement G_{FWM} increases toward the infrared part of the spectrum, reaching giant values $\sim 10^9$ at $\lambda \approx 1 \mu\text{m}$ (it keeps increasing further toward larger wavelengths). The increase with decreasing wavelength can be roughly approximated as $G_{FWM} \sim \lambda^q$, where $q = 2.2 \pm 0.2$. The dependence on the film size will be discussed below in the last subsection of this section. The above results indicate that semicontinuous films can be used, in particular, as a phase restoring material because of their high efficiency in the degenerate FWM resulting in the optical phase conjugation.

C. Third harmonic generation

We consider now higher harmonic generations in semi-continuous metal films under the action of the incident wave with frequency ω , and we begin with the third-harmonic generation (THG). The THG process is due to the third-order nonlinearity. The corresponding average nonlinear current that results in the generation of a signal with frequency 3ω has the form

$$\langle j_{3\omega\alpha}^{(3)}(\mathbf{r}) \rangle = \sigma_{3\omega e\alpha\beta\gamma\delta}^{(3)} E_{\omega\beta}^{(0)} E_{\omega\gamma}^{(0)} E_{\omega\delta}^{(0)}, \quad (54)$$

where $\mathbf{E}_\omega^{(0)}$ is the amplitude of the incident wave with frequency ω and $\sigma_{3\omega e\alpha\beta\gamma\delta}^{(3)}$ is the effective nonlinear conductivity. The nonlinear conductivity $\sigma_{3\omega e}^{(3)}$ for THG in an isotropic medium can be expressed in terms of only one independent constant so that the nonlinear current can be written as⁷² (see also discussion at the beginning of Sec. IV A)

$$\langle \mathbf{j}_{3\omega}^{(3)}(\mathbf{r}) \rangle = \sigma_{3\omega e}^{(3)} E_\omega^{(0)2} \mathbf{E}_\omega^{(0)}, \quad (55)$$

where $\sigma_{3\omega e}^{(3)}$ is the (scalar) nonlinear conductivity; frequencies of the fields and currents are shown in the subscripts.

We assume that adsorbed molecules with nonlinear conductivity $\sigma_{3\omega}^{(3)}(\mathbf{r})$ result in THG from a film. The local elec-

tric field $\mathbf{E}_\omega(\mathbf{r})$ excited in a film by the external field $\mathbf{E}_\omega^{(0)}$ generates the nonlinear current

$$\mathbf{j}_{s3\omega}^{(3)}(\mathbf{r}) = \sigma_{3\omega}^{(3)}(\mathbf{r}) E_\omega^2(\mathbf{r}) \mathbf{E}_\omega(\mathbf{r}), \quad (56)$$

with frequency 3ω , which flows in the layer of the adsorbed molecules. This current in turn interacts with the film and generates the ‘‘seed’’ electric field (at frequency 3ω) with the amplitude given by

$$\mathbf{E}_{3\omega}^{(3)}(\mathbf{r}) = \frac{\mathbf{j}_{s3\omega}^{(3)}(\mathbf{r})}{\sigma_{3\omega}^{(1)}(\mathbf{r})} = \left[\frac{\sigma_{3\omega}^{(3)}(\mathbf{r})}{\sigma_{3\omega}^{(1)}(\mathbf{r})} \right] E_\omega^2(\mathbf{r}) \mathbf{E}_\omega(\mathbf{r}), \quad (57)$$

where $\sigma_{3\omega}^{(1)}(\mathbf{r})$ is the *linear* conductivity of the adsorbed nonlinear molecule at the frequency 3ω . The electric field $\mathbf{E}_{3\omega}^{(3)}(\mathbf{r})$ can be thought of as an inhomogeneous external field that excites the film at the 3ω frequency. The THG current $\mathbf{j}_{3\omega}^{(3)}(\mathbf{r})$ generated in the film by the seed field $\mathbf{E}_{3\omega}^{(3)}(\mathbf{r})$ can be found now in terms of the nonlocal conductivity defined by Eq. (7) as

$$\mathbf{j}_{3\omega}^{(3)}(\mathbf{r}) = \int \hat{S}_{3\omega}(\mathbf{r}, \mathbf{r}') \mathbf{E}_{3\omega}^{(3)}(\mathbf{r}') d\mathbf{r}', \quad (58)$$

where $\hat{S}_{3\omega}$ is the nonlocal conductivity at frequency 3ω and the integration is over the entire film area. For the macroscopically isotropic films considered here the average THG current $\langle \mathbf{j}_{3\omega}^{(3)}(\mathbf{r}) \rangle$ is collinear with the average field $\mathbf{E}_{3\omega}^{(0)} = \langle \mathbf{E}_{3\omega}^{(3)}(\mathbf{r}) \rangle$. Thus we can write the average current in the form

$$\begin{aligned} \langle \mathbf{j}_{3\omega}^{(3)}(\mathbf{r}) \rangle &= \frac{\mathbf{E}_{3\omega}^{(0)}}{E_{3\omega}^{(0)2}} \langle [\mathbf{E}_{3\omega}^{(0)} \cdot \mathbf{j}_{3\omega}^{(3)}(\mathbf{r})] \rangle \\ &= \frac{\mathbf{E}_{3\omega}^{(0)}}{E_{3\omega}^{(0)2}} \frac{1}{A} \int \mathbf{E}_{3\omega}^{(0)} \hat{S}_{3\omega}(\mathbf{r}, \mathbf{r}') \mathbf{E}_{3\omega}^{(3)}(\mathbf{r}') d\mathbf{r} d\mathbf{r}', \end{aligned} \quad (59)$$

where the integrations are again over the entire area A of the film and $E_{3\omega}^{(0)2} \equiv (\mathbf{E}_{3\omega}^{(0)} \cdot \mathbf{E}_{3\omega}^{(0)})$. The integration over the coordinate \mathbf{r} gives

$$\langle \mathbf{j}_{3\omega}^{(3)}(\mathbf{r}) \rangle = \frac{\mathbf{E}_{3\omega}^{(0)}}{E_{3\omega}^{(0)2}} \langle \sigma_{3\omega}(\mathbf{r}) [\mathbf{E}_{3\omega}(\mathbf{r}) \cdot \mathbf{E}_{3\omega}^{(3)}(\mathbf{r})] \rangle, \quad (60)$$

where $\sigma_{3\omega}(\mathbf{r})$ is the linear film conductivity at frequency 3ω and $\mathbf{E}_{3\omega}(\mathbf{r})$ is the local field induced in the film by the uniform field $\mathbf{E}_{3\omega}^{(0)}$ oscillating with frequency 3ω .

When the frequency 3ω is within the band of plasmon resonances, i.e., $3\omega < \omega_p^*$ the field $\mathbf{E}_{3\omega}(\mathbf{r})$ is also a subject of giant fluctuations. Substituting in Eq. (60) the expression for the nonlinear field $\mathbf{E}_{3\omega}^{(3)}(\mathbf{r})$ defined in Eq. (57), we obtain the following equation for the THG current:

$$\langle \mathbf{j}_{3\omega}^{(3)}(\mathbf{r}) \rangle = \frac{\mathbf{E}_{3\omega}^{(0)}}{E_{3\omega}^{(0)2}} \left\langle \sigma_{3\omega}(\mathbf{r}) \left[\frac{\sigma_{3\omega}^{(3)}(\mathbf{r})}{\sigma_{3\omega}^{(1)}(\mathbf{r})} \right] [\mathbf{E}_{3\omega}(\mathbf{r}) \cdot \mathbf{E}_\omega(\mathbf{r})] E_\omega^2(\mathbf{r}) \right\rangle. \quad (61)$$

From this equation it follows that the average nonlinear current $\langle \mathbf{j}_{3\omega}^{(3)} \rangle$ resulting in the THG process can be expressed in terms of the *linear* local fields $\mathbf{E}_\omega(\mathbf{r})$ and $\mathbf{E}_{3\omega}(\mathbf{r})$ which are generated in the film by the uniform external fields $\mathbf{E}_\omega^{(0)}$ and $\mathbf{E}_{3\omega}^{(0)}$, respectively.

In the absence of metal grains, we can neglect the fluctuations and the fields $\mathbf{E}_\omega(\mathbf{r})$ and $\mathbf{E}_{3\omega}(\mathbf{r})$ coincide with the fields $\mathbf{E}_\omega^{(0)}$ and $\mathbf{E}_{3\omega}^{(0)}$, respectively. Therefore, for a film with no metal grains on it (but with nonlinear molecules), we find

$$\langle \mathbf{j}_{3\omega 0}^{(3)}(\mathbf{r}) \rangle = \mathbf{E}_{3\omega}^{(0)} \sigma_d \left[\frac{\sigma_{3\omega}^{(3)}(\mathbf{r})}{\sigma_{3\omega}^{(1)}(\mathbf{r})} \right] (\mathbf{E}_{3\omega}^{(0)} \cdot \mathbf{E}_\omega^{(0)}), \quad (62)$$

where $\sigma_d = -i\omega\varepsilon_d/4\pi$ is the film linear conductivity with no metal grains, i.e., the conductivity of the dielectric substrate.

As pointed out in the previous subsection, the nonlinear current (electric induction) should be averaged for coherent effects to find a signal from the system. The generated 3ω signal is proportional to the average current squared, $|\langle \mathbf{j}_{3\omega}^{(3)}(\mathbf{r}) \rangle|^2$. Accordingly, the factor characterizing the surface-enhanced THG is given by

$$G_{\text{THG}} = \frac{|\langle \mathbf{j}_{3\omega}^{(3)}(\mathbf{r}) \rangle|^2}{|\langle \mathbf{j}_{3\omega 0}^{(3)}(\mathbf{r}) \rangle|^2}. \quad (63)$$

As above, we assume that the adsorbed molecules possessing nonlinear conductivity cover the film homogeneously so that $\sigma_{3\omega}^{(1)}(\mathbf{r}) = \sigma_{3\omega}^{(1)}$ and $\sigma_{3\omega}^{(3)}(\mathbf{r}) = \sigma_{3\omega}^{(3)}$, i.e., both are \mathbf{r} independent. Then substituting Eqs. (61) and (62) into Eq. (63), we obtain the following equation for the enhancement G_{THG} of the THG process in semicontinuous metal films:

$$G_{\text{THG}} = \frac{\left| \frac{\langle \sigma_{3\omega}(\mathbf{r}) [\mathbf{E}_{3\omega}(\mathbf{r}) \cdot \mathbf{E}_\omega(\mathbf{r})] E_\omega^2(\mathbf{r}) \rangle}{\sigma_d (\mathbf{E}_{3\omega}^{(0)} \cdot \mathbf{E}_\omega^{(0)}) E_\omega^{(0)2}} \right|^2}{\left| \frac{\langle \varepsilon_{3\omega}(\mathbf{r}) [\mathbf{E}_{3\omega}(\mathbf{r}) \cdot \mathbf{E}_\omega(\mathbf{r})] E_\omega^2(\mathbf{r}) \rangle}{\varepsilon_d (\mathbf{E}_{3\omega}^{(0)} \cdot \mathbf{E}_\omega^{(0)}) E_\omega^{(0)2}} \right|^2}, \quad (64)$$

where $\sigma_{3\omega}(\mathbf{r})$, σ_d and $\varepsilon_{3\omega}(\mathbf{r})$, ε_d are the linear conductivities and dielectric functions of the film with and without metal grains, respectively (for clarity, we also indicate the frequencies ω and 3ω in the subscripts). The local fields in Eq. (64) resulting in the surface enhancement for the THG experience giant fluctuations in the spectral range corresponding to the plasmon resonances, i.e., for $\omega < \omega_p^*$, $3\omega > \omega_\tau$ (see discussion in Sec. III). This includes the optical, infrared, and far-infrared spectral ranges, where a huge enhancement of the THG can be observed in semicontinuous metal films.

When the frequency ω of the incident wave is large enough so that the third harmonic frequency 3ω is out of the spectral range of the plasmon resonances, i.e., $3\omega > \omega_p^*$, we can neglect the fluctuations of the 3ω field in Eq. (64) and this equation simplifies to

$$G_{\text{THG}} = \frac{|\langle \sigma_{3\omega}(\mathbf{r}) \mathbf{E}_\omega(\mathbf{r}) E_\omega^2(\mathbf{r}) \rangle|^2}{|\sigma_d|^2 |E_\omega^{(0)}|^6} = \frac{|\langle \varepsilon_{3\omega}(\mathbf{r}) \mathbf{E}_\omega(\mathbf{r}) E_\omega^2(\mathbf{r}) \rangle|^2}{\varepsilon_d^2 |E_\omega^{(0)}|^6}. \quad (65)$$

Note that in a macroscopically isotropic semicontinuous metal film the surface enhancements of the THG given by Eqs. (64) and (65) do not depend actually on the amplitude of the external field $\mathbf{E}_\omega^{(0)}$. The field $\mathbf{E}_{3\omega}^{(0)}$ in Eq. (64) is in a sense imaginary; it serves as a linear source of the fluctuating field $\mathbf{E}_{3\omega}(\mathbf{r})$ and the amplitude of the field $\mathbf{E}_{3\omega}^{(0)}$ can be chosen arbitrarily in calculations of the THG enhancement in Eqs. (64) and (65).

In Figs. 8 we show the average enhancements G_{THG} as functions of the wavelength which are calculated using Eqs. (65) and (64) [Figs. 8(a) and 8(b), respectively]. Note that in calculating the mean third and second harmonic signals we first found the generated intensity for each film separately and then averaged it over random samples. As for the processes considered above, the enhancements strongly increase toward larger wavelengths reaching at $\lambda \approx 3 \mu\text{m}$ the values $\sim 10^7$ and $\sim 10^5$, for the cases of Eqs. (64) and (65), respectively. The wavelength dependence of the THG enhancement in Eqs. (64) and (65) can be approximated as $G_{\text{THG}} \sim \lambda^q$, $q = 3.9 \pm 0.2$ and $G_{\text{THG}} \sim \lambda^q$, $q = 2.1 \pm 0.2$, respectively. (See also the discussion on the scaling in the dependence of G_{THG} on the film size given below.) Note that the enhancements for THG are significantly less than those in the case of four wave mixing, despite the fact that both processes are due to the same, third, order of nonlinearity. This is due to the partially destructive interference of the local fields at different points [see also the discussion accompanying Eq. (31)]. The magnitude of the enhancement in this case is smaller than that predicted by the upper limit in Eq. (31).

As follows from Eqs. (61) and (62), in the case when the generated field $\mathbf{E}_\omega(\mathbf{r})$ does not excite the plasmon resonances in the film and the 3ω field is uniform, $\mathbf{E}_{3\omega}(\mathbf{r}) = \mathbf{E}_{3\omega}^{(0)}$, the local currents $\mathbf{j}_{3\omega}^{(3)}(\mathbf{r})$ and $\mathbf{j}_{3\omega 0}^{(3)}(\mathbf{r})$ depend only on the local conductivities and fields at the same point \mathbf{r} . In the red and, especially, infrared parts of the spectrum, the distribution of $|\mathbf{j}_{3\omega}^{(3)}(\mathbf{r})|^2 \propto |\mathbf{E}_\omega(\mathbf{r}) E_\omega^2(\mathbf{r})|^2$ consists of spatially separated large peaks that can be probed independently by means of near-field scanning optical microscopy. This means that in this case we can consider the spatial distribution of the local third-harmonic signals $I_{3\omega}(\mathbf{r}) \propto |\mathbf{j}_{3\omega}^{(3)}(\mathbf{r})|^2$ and the local enhancements for THG defined as

$$g_{\text{THG}}(\mathbf{r}) = \frac{|\mathbf{j}_{3\omega}^{(3)}(\mathbf{r})|^2}{|\mathbf{j}_{3\omega 0}^{(3)}(\mathbf{r})|^2} = \frac{|\omega_{3\omega}(\mathbf{r})|^2}{|\sigma_d|^2} \frac{|\mathbf{E}_\omega(\mathbf{r}) E_\omega^2(\mathbf{r})|^2}{|E_\omega^{(0)} E_\omega^{(0)2}|^2}. \quad (66)$$

[We should note that since THG is a coherent process, the average enhancement G_{THG} cannot be found by simply averaging $g_{\text{THG}}(\mathbf{r})$.] In Fig. 9, we show the distribution $g_{\text{THG}}(\mathbf{r})$ for the surface-enhanced local THG signals at two different wavelengths, $\lambda = 0.5 \mu\text{m}$ and $\lambda = 1.5 \mu\text{m}$. We can see that the local THG signals consist of spatially separated sharp peaks, as expected. The local enhancements can be huge, up to 10^{13} , for the chosen wavelengths. The spatial

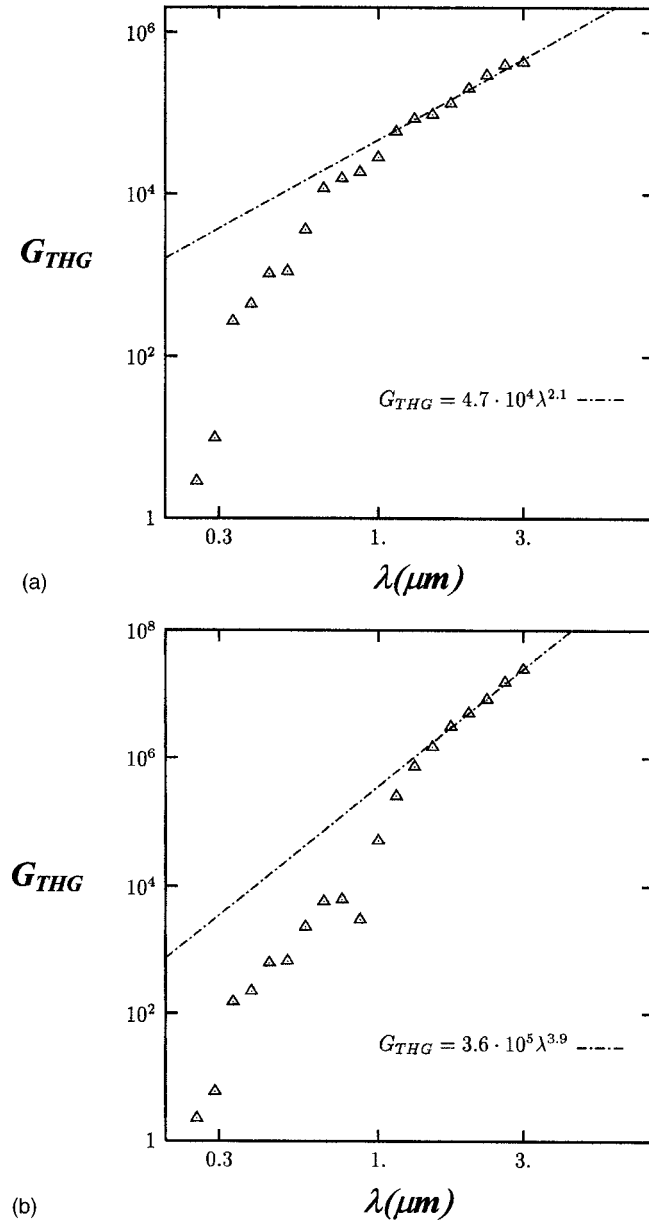


FIG. 8. The average THG enhancement G_{THG} on a silver semi-continuous film as a function of the wavelength at $p = p_c$. (a) No additional enhancement associated with the excitation of the film resonances at 3ω ; (b) the additional enhancement is included. The film sizes are 512×512 .

positions of the hot zones for the local nonlinear scattering associated with THG are very sensitive to the frequency of the incident light. We emphasize again that the enhancements in the peaks significantly exceed the average background enhancement. As above, the reason for this is, in part, the destructive interference between generated fields in different points, and, in part, the fact that the peaks are separated by distances significantly larger than their spatial sizes.

For a frequency-degenerate coherent process, such as DFWM, one cannot find the local enhancement in such a simple way as above. Also we note that for frequency-degenerate nonlinear processes on random semicontinuous films one probably cannot distinguish in experiment the local nonlinear field from the local linear field at the same point; this is because both linear and nonlinear fields have the same

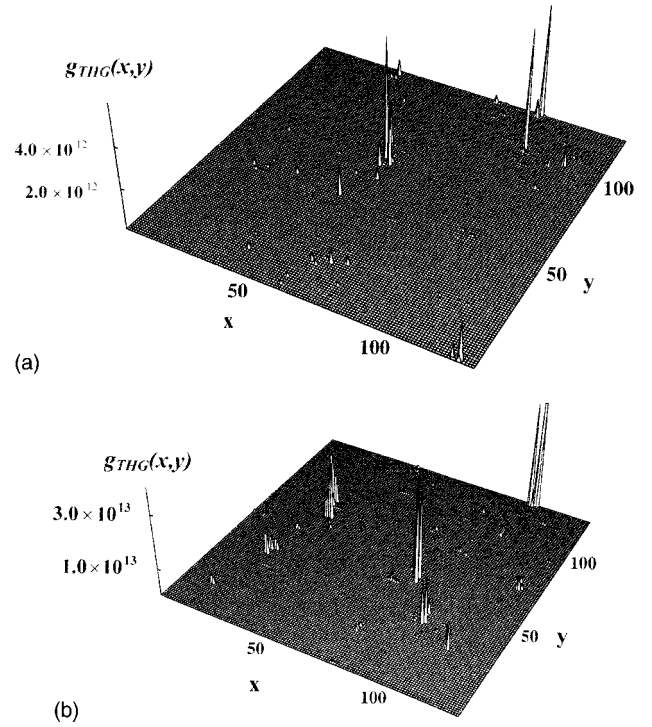


FIG. 9. Spatial distributions of the local THG enhancements $g_{THG}(\mathbf{r})$ for $\lambda = 0.5 \mu\text{m}$ (a) and $\lambda = 1.5 \mu\text{m}$ (b) at $p = p_c$.

frequency. However, this is not the case for nearly degenerate FWM, when all the waves have slightly different frequencies and the enhancements are especially large.

There is no simple formula for the local THG signal when the frequency of the third harmonic is less than the renormalized plasma frequency $3\omega < \omega_p^*$. In this case, the THG amplitudes excite the giant field fluctuations at 3ω frequency, so that the THG field experience the additional enhancement considered above. Still, in this case, we can also anticipate highly localized sharp peaks for the local field intensities at frequency 3ω that can be probed using the methods of near-field optics.

D. Second harmonic generation

Second harmonic generation (SHG) is a nonlinear process resulting in the generation of the signal at double frequency 2ω when light with frequency ω is incident on a system. The second harmonic wave is generated due to the nonlinear current $\mathbf{j}^{(2)}(2\omega)$ which is expressed in terms of the amplitude of the macroscopic field $\mathbf{E}^{(0)}(\omega)$ at fundamental frequency ω as

$$j_{\alpha}^{(2)}(2\omega) = \sigma_{e\alpha\beta\gamma}^{(2)}(2\omega) E_{\beta}^{(0)}(\omega) E_{\gamma}^{(0)}(\omega), \quad (67)$$

where $\sigma_{e\alpha\beta\gamma}^{(2)}(2\omega)$ is the tensor of the effective nonlinear conductivity responsible for the SHG process. (Note that in this subsection we put frequencies in the arguments of the considered quantities to avoid awkward indices.) The existence of the SHG conductivity applies some restrictions on the symmetry of the system. For example, the tensor of the nonlinear conductivity is equal to zero for centrosymmetric media.⁷² As a result, a relation between the SHG current and microscopic fields cannot be reduced to a simple vector form as in the case of the THG and FWM processes considered

above. [Note that usually the phenomenon of SHG is described in terms of the nonlinear dielectric function $\varepsilon^{(2)} = i4\pi\sigma^{(2)}/(2\omega)$;⁷² however, we will keep the concept of nonlinear currents and conductivities chosen for this paper, which is completely equivalent to the concept of nonlinear polarizations and dielectric functions (susceptibilities).]

We will assume that a semicontinuous metal film, which is macroscopically homogeneous and isotropic, is covered by a layer of the SHG-active molecules. Then the local electric field $\mathbf{E}(\omega, \mathbf{r})$ excited by the external field $\mathbf{E}^{(0)}(\omega)$ generates linear and nonlinear currents $\mathbf{j}^{(1)}(\omega, \mathbf{r})$ and $\mathbf{j}^{(2)}(2\omega, \mathbf{r})$ in the adsorbed molecules. The nonlinear current is expressed in terms of the local field $\mathbf{E}(\omega, \mathbf{r})$ in the following way:

$$j_{s,\alpha}^{(2)}(2\omega, \mathbf{r}) = \sigma_{\alpha\beta\gamma}^{(2)}(2\omega) E_{\beta}(\omega, \mathbf{r}) E_{\gamma}(\omega, \mathbf{r}), \quad (68)$$

where $\sigma_{\alpha\beta\gamma}^{(2)}(2\omega)$ is the nonlinear conductivity of the molecule layer which is responsible for SHG. For the sake of simplicity, we assume that the SHG molecules cover a semicontinuous metal film uniformly and, therefore, the linear and nonlinear conductivities of the molecular layer $\sigma^{(1)}$ and $\sigma^{(2)}$ are independent of the coordinate \mathbf{r} in the film plane. We also assume that the linear conductivity $\sigma^{(1)}$ is a scalar. The nonlinear current given by Eq. (68) excites the seed electric field with frequency 2ω ,

$$E_{s\alpha}^{(2)}(2\omega, \mathbf{r}) = \frac{j_{s\alpha}^{(2)}(2\omega, \mathbf{r})}{\sigma^{(1)}(2\omega)} = \left[\frac{\sigma_{\alpha\beta\gamma}^{(2)}(2\omega)}{\sigma^{(1)}(2\omega)} \right] E_{\beta}(\omega, \mathbf{r}) E_{\gamma}(\omega, \mathbf{r}), \quad (69)$$

where $\sigma^{(1)}(2\omega)$ is the *linear* conductivity of the adsorbed molecules at frequency 2ω , which is assumed to be a scalar. We consider the electric field $\mathbf{E}_s^{(2)}(2\omega, \mathbf{r})$ as an external non-uniform electric field that excites the local current $\mathbf{j}^{(2)}(2\omega, \mathbf{r})$ in a semicontinuous film at frequency 2ω . This current can be found using the nonlocal conductivity matrix defined by Eq. (7); this gives

$$\begin{aligned} j_{\alpha}^{(2)}(2\omega, \mathbf{r}) &= \int S_{\alpha\beta}(2\omega, \mathbf{r}, \mathbf{r}') E_{s\beta}^{(2)}(2\omega, \mathbf{r}') d\mathbf{r}' \\ &= \int S_{\alpha\beta}(2\omega, \mathbf{r}, \mathbf{r}') \\ &\quad \times \left[\frac{\sigma_{\beta\gamma\delta}^{(2)}(2\omega)}{\sigma^{(1)}(2\omega)} \right] E_{\gamma}(\omega, \mathbf{r}') E_{\delta}(\omega, \mathbf{r}'), d\mathbf{r}', \end{aligned} \quad (70)$$

where the integration is over the entire area A of the film. As above, the summation over the repeating Greek indices (which take values 1 and 2 in the considered 2D case) is implied. The second equality in the above equation is obtained by substituting the field $E_{s\beta}^{(2)}(2\omega, \mathbf{r})$ from Eq. (69). Now we introduce the uniform probe field

$$\mathbf{E}^{(0)}(2\omega) = \langle \mathbf{E}_s^{(2)}(2\omega, \mathbf{r}) \rangle, \quad (71)$$

where $\langle \dots \rangle$ denotes, as above, the average over the film area A . Since we consider macroscopically isotropic semicontinuous films the average nonlinear current $\langle \mathbf{j}^{(2)}(2\omega, \mathbf{r}) \rangle$ has the same direction as the field $\mathbf{E}^{(0)}(2\omega)$, and it can be written as

$$\langle \mathbf{j}^{(2)}(2\omega, \mathbf{r}) \rangle = \frac{\mathbf{E}^{(0)}(2\omega)}{E^{(0)2}(2\omega)} \langle [\mathbf{E}^{(0)}(2\omega) \cdot \mathbf{j}^{(2)}(2\omega, \mathbf{r})] \rangle. \quad (72)$$

Substituting in the above equation the expression for the current $\mathbf{j}^{(2)}(2\omega, \mathbf{r})$ from Eq. (70), we obtain

$$\begin{aligned} \langle \mathbf{j}^{(2)}(2\omega, \mathbf{r}) \rangle &= \frac{\mathbf{E}^{(0)}(2\omega)}{E^{(0)2}(2\omega)} \left\langle \int E_{\alpha}^{(0)}(2\omega) S_{\alpha\beta}(2\omega, \mathbf{r}, \mathbf{r}') \right. \\ &\quad \times \left. \left[\frac{\sigma_{\beta\gamma\delta}^{(2)}(2\omega)}{\sigma^{(1)}(2\omega)} \right] E_{\gamma}(\omega, \mathbf{r}') E_{\delta}(\omega, \mathbf{r}'), d\mathbf{r}' \right\rangle \\ &= \frac{\mathbf{E}^{(0)}(2\omega)}{E^{(0)2}(2\omega)} \frac{1}{A} \int E_{\alpha}^{(0)}(2\omega) S_{\alpha\beta}(2\omega, \mathbf{r}, \mathbf{r}') \\ &\quad \times \left[\frac{\sigma_{\beta\gamma\delta}^{(2)}(2\omega)}{\sigma^{(1)}(2\omega)} \right] E_{\gamma}(\omega, \mathbf{r}') E_{\delta}(\omega, \mathbf{r}'), d\mathbf{r}, d\mathbf{r}', \end{aligned} \quad (73)$$

where both integrations are over the film area A . Integrating Eq. (73) over \mathbf{r} and using the symmetry of the nonlocal conductivity [see Eq. (9) and the accompanying discussion], we obtain

$$\begin{aligned} \langle \mathbf{j}^{(2)}(2\omega, \mathbf{r}) \rangle &= \frac{\mathbf{E}^{(0)}(2\omega)}{E^{(0)2}(2\omega)} \frac{1}{A} \int \sigma(2\omega, \mathbf{r}) E_{\alpha}(2\omega, \mathbf{r}) \\ &\quad \times \left[\frac{\sigma_{\alpha\beta\gamma}^{(2)}(2\omega)}{\sigma^{(1)}(2\omega)} \right] E_{\gamma}(\omega, \mathbf{r}) E_{\delta}(\omega, \mathbf{r}) d\mathbf{r} \\ &= \frac{\mathbf{E}^{(0)}(2\omega)}{E^{(0)2}(2\omega)} \left\langle \sigma(2\omega, \mathbf{r}) E_{\alpha}(2\omega, \mathbf{r}) \right. \\ &\quad \times \left. \left[\frac{\sigma_{\alpha\beta\gamma}^{(2)}(2\omega)}{\sigma^{(1)}(2\omega)} \right] E_{\beta}(\omega, \mathbf{r}) E_{\gamma}(\omega, \mathbf{r}) \right\rangle, \end{aligned} \quad (74)$$

where the field $\mathbf{E}_{\alpha}(2\omega, \mathbf{r})$ is the local field excited in the film by the uniform external field $\mathbf{E}^{(0)}(2\omega)$ and $\sigma(2\omega, \mathbf{r})$ is the (linear) local film conductivity at the second harmonic frequency.

For the following consideration it is instructive to present the local fields as $\mathbf{E}(\omega) = \mathbf{e}_1(\omega) E(\omega)$ and $\mathbf{E}(2\omega) = \mathbf{e}_2(2\omega) E(2\omega)$, where \mathbf{e}_1 and \mathbf{e}_2 are real unit vectors of polarization [$(\mathbf{e}_1 \cdot \mathbf{e}_1) = 1$, $(\mathbf{e}_2 \cdot \mathbf{e}_2) = 1$]. Then Eq. (74) can be rewritten in the form

$$\begin{aligned} \langle \mathbf{j}^{(2)}(2\omega, \mathbf{r}) \rangle &= \frac{\mathbf{E}^{(0)}(2\omega)}{E^{(0)2}(2\omega)} \\ &\quad \times \langle \sigma(2\omega, \mathbf{r}) \eta(\omega, \mathbf{r}) E(2\omega, \mathbf{r}) E^2(\omega, \mathbf{r}) \rangle, \end{aligned} \quad (75)$$

where the function $\eta(\omega, \mathbf{r})$ is defined as

$$\eta(\omega, \mathbf{r}) = \left[\frac{\sigma_{\alpha\beta\gamma}^{(2)}(2\omega)}{\sigma^{(1)}(2\omega)} \right] e_{2\alpha}(2\omega, \mathbf{r}) e_{1\beta}(\omega, \mathbf{r}) e_{1\gamma}(\omega, \mathbf{r}). \quad (76)$$

Since all fluctuating quantities in Eq. (76) are of the order of unity it is plausible to suggest that the function $\eta(\mathbf{r})$ fluctuates over the film much less than the local field amplitudes $E(\omega, \mathbf{r})$ and $E(2\omega, \mathbf{r})$. There is also no reason for the zeros of the function $\eta(\mathbf{r})$ to coincide systematically with the maxima of the amplitudes. Therefore, for the estimation of the order of magnitude one can use the decoupling procedure and replace $\eta(\omega, \mathbf{r})$ by its average value which we denote as $\tilde{\eta}(\omega) = \langle \eta(\omega, \mathbf{r}) \rangle$. Then Eq. (75) for the second-harmonic current acquires the simple form

$$\langle \mathbf{j}^{(2)}(2\omega, \mathbf{r}) \rangle = \frac{\mathbf{E}^{(0)}(2\omega)}{\mathbf{E}^{(0)2}(2\omega)} \tilde{\eta}(\omega) \times \langle \sigma(2\omega, \mathbf{r}) E(2\omega, \mathbf{r}) E^2(\omega, \mathbf{r}) \rangle. \quad (77)$$

In the absence of metal grains there are no local field fluctuations. Under the same assumption, as above the nonlinear current is equal to

$$\mathbf{j}^{(20)}(2\omega) = \frac{\mathbf{E}^{(0)}(2\omega)}{\mathbf{E}^{(0)2}(2\omega)} \eta_0(\omega) \sigma_d E^{(0)}(2\omega) E^{(0)2}(\omega), \quad (78)$$

where $\eta_0(\omega) = [\sigma_{\alpha\beta\gamma}^{(2)}/\sigma^{(1)}] e_{20\alpha} e_{10\beta} e_{10\gamma}$, and \mathbf{e}_{10} and \mathbf{e}_{20} are the unit vectors of the polarization of the fields $\mathbf{E}^{(0)}(\omega)$ and $\mathbf{E}^{(0)}(2\omega)$, respectively.

The enhancement factor for SHG is given by the modulus squared of the ratio of the average nonlinear currents with and without metal grains [cf. Eq. (63)] $G_{\text{SHG}} = |\langle \mathbf{j}^{(2)}(2\omega, \mathbf{r}) \rangle|^2 / |\mathbf{j}_0^{(2)}(2\omega)|^2$. Assuming that the ratio $\tilde{\eta}/\eta_0$ is of the order of unity we obtain the following estimate for the SHG enhancement:

$$G_{\text{SHG}} \sim \frac{|\langle \sigma(2\omega, \mathbf{r}) E^2(\omega, \mathbf{r}) E(2\omega, \mathbf{r}) \rangle|^2}{|\sigma_d|^2 |\mathbf{E}^{(0)}(\omega)|^4 |\mathbf{E}^{(0)}(2\omega)|^2}. \quad (79)$$

In the case when the second harmonic frequency is above the renormalized plasma frequency, i.e., $2\omega > \omega_p^*$ [Eq. (2)] the local field fluctuations can be neglected at frequency 2ω . Then the local field $\mathbf{E}(2\omega, \mathbf{r}) \approx \mathbf{E}^{(0)}(2\omega)$ and the surface enhancement for SHG simplifies to

$$G_{\text{SHG}} \sim \frac{|\langle \sigma(2\omega, \mathbf{r}) E^2(\omega, \mathbf{r}) \rangle|^2}{|\sigma_d|^2 |\mathbf{E}^{(0)}(\omega)|^4}. \quad (80)$$

The enhancement of the SHG process given by Eqs. (79) and (80) does not depend on the amplitudes of the fields $\mathbf{E}^{(0)}(\omega)$ and $\mathbf{E}^{(0)}(2\omega)$ for the macroscopically homogeneous and isotropic random semicontinuous films considered here. These fields can be taken as arbitrary for the computer simulation of the local fields $\mathbf{E}(\omega, \mathbf{r})$ and $\mathbf{E}(2\omega, \mathbf{r})$ excited by $\mathbf{E}^{(0)}(\omega)$ and $\mathbf{E}^{(0)}(2\omega)$.

In Figs. 10(a) and 10(b), the average enhancements G_{SHG} found from Eqs. (80) and (79) are shown as functions of the wavelength. (As above, $p = p_c$, the film sizes are 512×512 , and the results were averaged over 100 realizations of the system). As seen in the figure, the enhancement increases toward the infrared part of the spectrum reaching values $\sim 10^4$ and $\sim 10^6$ at $\lambda \approx 3 \mu\text{m}$, in the first and second cases, respectively. The corresponding wavelength dependencies

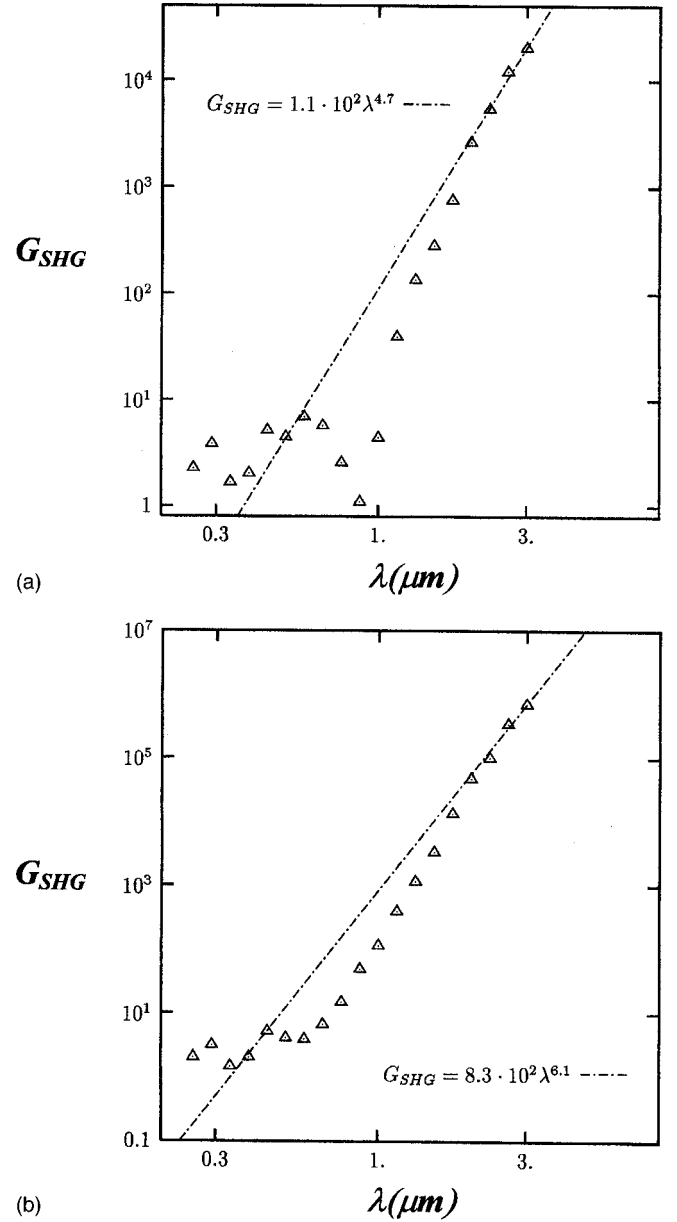


FIG. 10. The average SHG enhancement G_{SHG} on a silver semicontinuous film as a function of the wavelength at $p = p_c$. (a) No additional enhancement due to excitation of the film resonances at 2ω ; (b) the additional enhancement is included. The film sizes are 512×512 .

can be approximated by power-law expressions with indices 4.7 ± 0.3 and 6.1 ± 0.4 , for the above two cases.

Similar to the consideration of the local THG in the previous subsection, we can calculate spatial distributions of the local SHG signals, provided that the generated frequency is outside of the film resonance band, so that the local current $\mathbf{j}^{(2)}(2\omega, \mathbf{r})$ depends only on the local conductivities and fields taken at the same point \mathbf{r} . As above, in the red and, especially, infrared parts of the spectrum, the distribution of $|\mathbf{j}^{(2)}(2\omega, \mathbf{r})|^2 \propto |\mathbf{E}(2\omega, \mathbf{r})|^2$ consists of very large spatially separated peaks, which can be probed independently by means of near-field scanning optical microscopy. Thus, it is important to consider the spatial distributions of the local SHG signals $I_{2\omega}(\mathbf{r}) \propto |\mathbf{j}^{(2)}(2\omega, \mathbf{r})|^2$ and the local enhancements for SHG, defined as

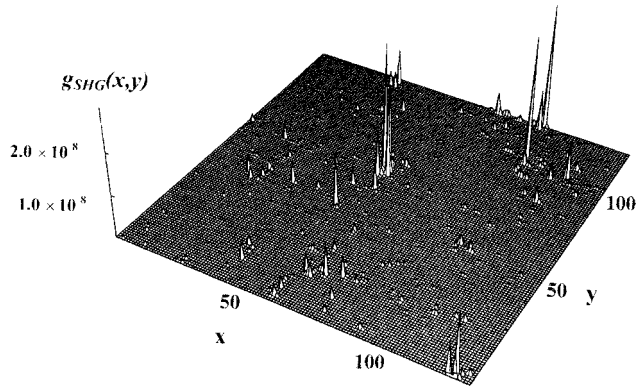


FIG. 11. Spatial distributions of the local SHG enhancements $g_{\text{SHG}}(\mathbf{r})$ for $\lambda = 0.5 \mu\text{m}$ at $p = p_c$.

$$g_{\text{SHG}}(\mathbf{r}) = \frac{|\sigma(2\omega, \mathbf{r})|^2 |\mathbf{E}(\omega, \mathbf{r})|^4}{|\sigma_d|^2 |\mathbf{E}^{(0)}(\omega)|^4}. \quad (81)$$

In Fig. 11 we show the SHG distribution $g_{\text{SHG}}(\mathbf{r})$ at $\lambda = 0.5 \mu\text{m}$. We can see that the local SHG signals are formed by spatially separated sharp peaks. The local enhancements can be huge, up to 10^8 . It is interesting to note that the average enhancement for SHG is small; at $\lambda = 0.5 \mu\text{m}$ it is only of the order of 10, whereas the local enhancements can be very large. As in the case of the THG process, this is due to the destructive interference of the fields generated from different points of the film and large spatial separations of the peaks. The spatial positions of the hot zones for the local SHG signal are sensitive to the incident wave frequency, which is the same as for the above considered nonlinear processes.

Note that when SHG is very efficient, the energy associated with the nonlinear current $\mathbf{j}(2\omega)$ can be transformed back to $\mathbf{j}(\omega)$ due to the same nonlinear conductivity $\sigma^{(2)}$ which provides the SHG. This would result in nonlinear corrections to the absorption and refraction, an effect which was described above in terms of the third-order nonlinear conductivity $\sigma^{(3)}$ responsible for the Kerr effect. This is an example of the so-called cascaded nonlinearities that simulate with $\sigma^{(2)}$ the optical effects typically associated with $\sigma^{(3)}$.⁷³ This phenomenon is very important for a number of applications in nonlinear optics, such as $\sigma^{(2)}$ -based materials for optical switches and soliton localization.⁷³ Semicontinuous metal films providing very strong enhancements for second-order optical nonlinearities can be considered as candidates for advanced optical materials with large cascaded nonlinearities.

In our above calculations of the optical nonlinearities we used samples of the same size, 512×512 . Below, we show that the enhancements for nonlinear optical processes scales with the film size.

E. Size-effects for nonlinear optical processes on a semicontinuous film

Different peaks in the field distributions (see, for example, Fig. 3) correspond to the fields that can have correlated phases and therefore can interfere. This implies that there may be a characteristic phase-coherence length l_p which is larger than or comparable to the size of the film. In this case,

the enhancement is anticipated to depend on the film size. In Fig. 12, we show results of our calculations of enhancements for the nonlinear optical processes performed for different film sizes. We used three different ensembles in these calculations consisting of 100 samples of 512×512 size, 400 samples of 256×256 size, and 1600 samples of 128×128 sizes. In Fig. 12, we plot the ‘‘scaled’’ enhancements $G^{(n)}(L)(L/L_0)^\alpha$, where $L_0 = 512$ as in the above calculations (the results shown with triangles), $L = 256$ (circles), and $L = 128$ (crosses). The following nonlinear processes are shown in the figure: 12(a) FWM ($\alpha = 2.2$ was used to collapse the data on the same curve); 12(b) and 12(c): THG with and without the ‘‘additional’’ enhancement at the generated frequency 3ω ($\alpha = 2.1$ and $\alpha = 2.0$ were used, respectively); 12(d) and 12(e): SHG with and without the ‘‘additional’’ enhancement at the generated frequency 2ω ($\alpha = 2.0$ for both cases). Similar calculations for the enhanced Kerr nonlinearity (not shown) give $\alpha = 1.1$ for $|G'_K|$, $\alpha = 0.7$ for $G''_K > 0$, and $\alpha = 1.4$ for $G''_K < 0$. (Note that for G_K the calculations show large deviations of the average values.) The above indicated values of α were used to provide the best collapse of the data for different sizes L . However, within the standard deviation, all the results can be roughly expressed as

$$G^{(n)} \propto L^{-2}, \quad (82)$$

for parametric processes, such as FWM and THG ($n = 3$), and SHG ($n = 2$), and

$$G_K \propto L^{-1} \quad (83)$$

for the nonparametric process, such as nonlinear refraction and absorption described by the Kerr susceptibility.

We should stress that the number of different sizes of the semicontinuous metal film ($L = 128, 256, 512$) investigated by the computer experiment is not enough to make definite conclusions about the indexes α or to attempt to develop some L - λ scaling for the enhancements of the various nonlinearities originating from the giant fluctuations of the local field in the films. Yet the above results can be considered as an indication that there is a destructive (in part) interference between the well-separated peaks in the field distributions; these peaks often represent morphologically disconnected parts of the same antisymmetric (or partially antisymmetric) mode, so that their contributions cancel each other in part. Also, we can conclude that the phase-coherence length is comparable or larger than the size of the samples used in our calculations. Because Raman scattering is a local effect and the enhancement given by Eq. (50) depends only on the field magnitudes (but not their phases), the enhancement for Raman scattering does not depend on the size of the sample. This was verified in our simulations (not shown).

We also note that the above results on the size effect for the enhanced nonlinear optical processes in a semicontinuous film are different from those obtained previously in fractals.²¹ For fractals, because of the localization of the modes, different hot spots in most cases are not phase correlated, and the enhancements do not depend on the size of the sample. To verify this, we recently performed calculations (similar to those described in Ref. 21) for fractal small-particle aggregates and for self-affine films with very differ-

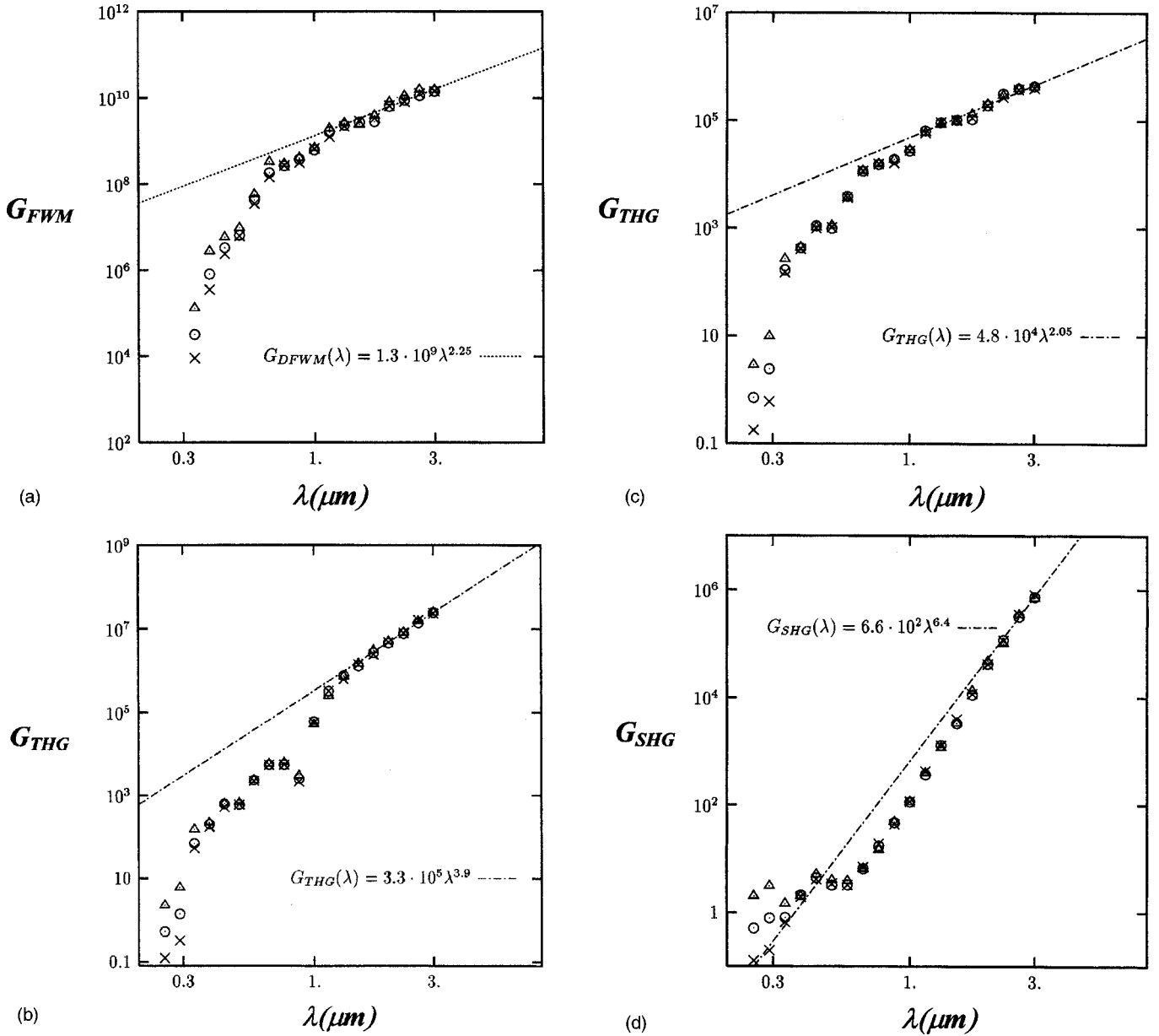


FIG. 12. The “scaled” enhancements $G^{(n)}(L)(L/L_0)^\alpha$ for various nonlinear optical processes. $L_0=512$ (triangles), $L=256$ (circles), and $L=128$ (crosses). (a) FWM ($\alpha=2.2$), (b) THG with an additional enhancement at 3ω ($\alpha=2.1$), (c) THG with no additional enhancement ($\alpha=2.0$), (d) SHG with an additional enhancement at 2ω ($\alpha=2.0$), and (e) SHG with no additional enhancement ($\alpha=2.0$).

ent sizes; the calculations showed that in fractals there is no size effect similar to the one described above for semicontinuous metal films, at least for fractal samples with the number of particles up to $N=10\,000$ used in our simulation.

V. CONCLUSIONS

In this paper we studied surface-enhanced optical nonlinearities of random metal-dielectric films (also referred to throughout the text as semicontinuous films). We showed that electric fields in such films consist of localized sharp peaks resulting in very inhomogeneous spatial distributions of local fields. In peaks (hot spots), the local fields exceed the applied field by several orders of magnitudes. These peaks are localized in nm-sized areas and can be associated with the plasmon modes of metal clusters formed in a semicontinuous film. For any particular frequency in the visible

infrared and far-infrared spectral ranges we can find a family of metal clusters so that each cluster from the family possesses a plasmon resonance. The amount of metal grains comprising these resonance clusters is negligibly small in comparison with the total number of metal grains. Nevertheless, the resonance clusters densely cover the entire surface of the film due to their fractality. The incident light excites the resonance clusters and they interact with each other. As a result, the local field is concentrated in sharp peaks placed in some subset of the resonance clusters. The amplitudes of the peaks and the average distances between them increase towards the infrared.

The strongly fluctuating fields associated with the sharp peaks in various random parts of a film, result in giant enhancements of nonlinear optical processes since they are proportional to the enhanced local fields raised to a power higher than 1. Because of such a pattern for the local field

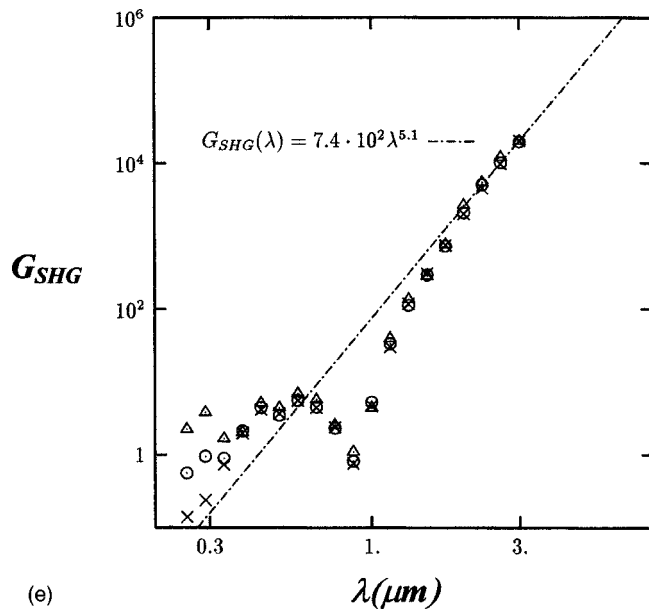


FIG. 12. (Continued).

distribution, the nonlinear signal is mostly generated from very small nm-sized areas. The corresponding spatial distributions for the generated fields also look similar to a set of very sharp peaks (actually, even sharper than those for the field at fundamental frequency). The enhancement in these peaks is much larger (by several orders of magnitude) than the ensemble-average enhancement because the peaks are separated by distances much larger than the peak sizes which are comparable with the metal grain sizes. Another important reason is related to the fact that the well-separated peaks are represented as being often disconnected in space parts of the same mode and, therefore, are correlated in phase. Destruc-

tive (in part) interference between the local fields in different parts of the film results in the decreased average enhancements. Note that the latter mechanism of the destructive interference is not important for incoherent processes, such as Raman scattering. Both the local and average enhancements for nonlinear optical processes strongly increase toward the long-wavelength part of the spectrum.

Since the applied (fundamental) and generated fields have, in general, different frequencies and polarizations, they excite different eigenmodes of the film so that the field spatial distributions for the fundamental and generated waves are different as well. Accordingly, the spatial positions of the hot spots at the fundamental and generated frequencies are located, in general, in different parts of a film. This picture is expected to be typical for various optical processes in strongly disordered systems,^{32,35} such as the random semi-continuous films studied here (similar field patterns also occur, for example, in metal fractal aggregates²¹ and self-affine thin films²⁴). Specifically, hot spots associated with fields at different frequencies and polarizations are localized in spatially separated nm-sized areas. Note also that because the hot spots are localized in nm-sized areas and provide giant enhancement in their locations, a fascinating possibility of *nonlinear* spectroscopy of single molecules on a semicontinuous metal film becomes feasible. These nano-optical effects can be probed, for example, with near-field scanning optical microscopy providing subwavelength spatial resolution.

ACKNOWLEDGMENTS

This research was supported in part by NSF Grant No. DMR-9500258 and NATO Grant No. CRG-950097. Acknowledgment is also made to the donors of The Petroleum Research Fund, administered by the ACS, for partial support of this research.

- ¹L. de Arcangelis, S. Redner, and H. J. Herrmann, *J. Phys. (France) Lett.* **46**, L585 (1985).
- ²P. M. Duxbury, P. L. Leath, and P. D. Beale, *Phys. Rev. B* **36**, 367 (1987).
- ³B. Khang, G. G. Batrouni, S. Redner, L. de Arcangelis, and H. J. Herrmann, *Phys. Rev. B* **37**, 7625 (1988).
- ⁴A. P. Vinogradov, A. V. Goldenshtein, and A. K. Sarychev, *Zh. Tekh. Fiz.* **59**, 208 (1989).
- ⁵*Statistical Models for the Fracture of Disordered Media*, edited by H. J. Herrmann and S. Roux (Elsevier, British Vancouver, 1990); P. Meakin, *Science* **252**, 226 (1991); P. M. Duxbury and P. L. Leath, *Phys. Rev. B* **49**, 12 676 (1994), and references therein.
- ⁶K. K. Bardhan and R. K. Chakrabarty, *Phys. Rev. Lett.* **72**, 1068 (1994); U. N. Nandi and K. K. Bardhan, *Europhys. Lett.* **31**, 101 (1995); K. K. Bardhan, *Physica A* **241**, 267 (1997).
- ⁷A. K. Sarychev and F. Brouers, *Phys. Rev. Lett.* **73**, 2895 (1994).
- ⁸A. Aharony, *Phys. Rev. Lett.* **58**, 2726 (1987).
- ⁹D. Stroud and P. M. Hui, *Phys. Rev. B* **37**, 8719 (1988).
- ¹⁰V. M. Shalaev and M. I. Shtockman, *Zh. Éksp. Teor. Fiz.* **92**, 509 (1987) [*Sov. Phys. JETP* **65**, 287 (1987)]; A. V. Butenko, V. M. Shalaev, and M. I. Shtockman, *ibid.* **94**, 107 (1988) [*ibid.* **67**, 60 (1988)].
- ¹¹D. J. Bergman, *Phys. Rev. B* **39**, 4598 (1989).
- ¹²D. J. Bergman and D. Stroud, *Solid State Phys.* **46**, 14 (1992).
- ¹³P. M. Hui, in *Nonlinearity and Breakdown in Soft Condensed Matter*, edited by K. K. Bardhan, B. K. Chakrabarty, and A. Hansen, Vol. 437 of *Lecture Notes in Physics* (Springer, Berlin, 1996).
- ¹⁴V. M. Shalaev, *Phys. Rep.* **272**, 61 (1996).
- ¹⁵D. Bergman, O. Levy, and D. Stroud, *Phys. Rev. B* **49**, 129 (1994); O. Levy and D. Bergman, *Physica A* **207**, 157 (1994); O. Levy, D. J. Bergman, and D. G. Stroud, *Phys. Rev. E* **52**, 3184 (1995).
- ¹⁶R. W. Cohen, G. D. Cody, M. D. Coutts, and B. Abeles, *Phys. Rev. B* **8**, 3689 (1973).
- ¹⁷J. P. Clerc, G. Giraud, and J. M. Luck, *Adv. Phys.* **39**, 191 (1990).
- ¹⁸C. Flytzanis, *Prog. Opt.* **29**, 2539 (1992), and references therein.
- ¹⁹A. V. Butenko, P. A. Chubakov, Yu. E. Danilova, S. V. Karpov, A. K. Popov, S. G. Rautian, V. P. Safonov, V. V. Slabko, V. M. Shalaev, and M. I. Stockman, *Z. Phys. D* **17**, 283 (1990); Yu. E. Danilova, S. G. Rautian, V. P. Safonov, P. A. Chubakov, V. M. Shalaev, and M. I. Shtockman, *Pis'ma Zh. Éksp. Teor. Fiz.* **47**, 200 (1988) [*JETP Lett.* **47**, 243 (1988)]; Yu. E. Danilova, V. P. Drachev, S. V. Perminov, and V. P. Safonov, *Izv. Ross. Akad.*

- Nauk, Ser. Fiz. **60**, 18 (1996); **60**, 56, (1996); Bull. Russ. Acad. Sci. **60**, 342 (1996); Yu. E. Danilova, S. G. Rautian, and V. P. Safonov, *ibid.* **60**, 374 (1996).
- ²⁰V. M. Shalaev, M. I. Stockman, and R. Botet, *Physica A* **185**, 181 (1992); V. M. Shalaev, V. A. Markel, and V. P. Safonov, *Fractals* **2**, 201 (1994); V. M. Shalaev *et al.*, *Physica A* **207**, 197 (1994); V. M. Shalaev, E. Y. Poliakov, V. A. Markel, and R. Botet, *ibid.* **241**, 249 (1997).
- ²¹V. M. Shalaev, E. Y. Poliakov, and V. A. Markel, *Phys. Rev. B* **53**, 2437 (1996); V. A. Markel, V. M. Shalaev, E. B. Stechel, W. Kim, and R. L. Armstrong, *ibid.* **53**, 2425 (1996).
- ²²M. I. Stockman, L. N. Pandey, L.S. Muratov, and T. F. George, *Phys. Rev. Lett.* **72**, 2486 (1994); *Phys. Rev. B* **51**, 185 (1995); M. I. Stockman, L. N. Pandey, and T. F. George, *ibid.* **53**, 2183 (1996).
- ²³V. M. Shalaev, R. Botet, and A. V. Butenko, *Phys. Rev. B* **48**, 6662 (1993); D. P. Tsai, J. Kovacs, Z. Wang, M. Moskovits, V. M. Shalaev, J. Suh, and R. Botet, *Phys. Rev. Lett.* **72**, 4149 (1994); V. M. Shalaev and M. Moskovits, *ibid.* **75**, 2451 (1995).
- ²⁴V. M. Shalaev, R. Botet, J. Mercer, and E. B. Stechel, *Phys. Rev. B* **54**, 8235 (1996); E. Y. Poliakov, V. M. Shalaev, V. M. Markel, and R. Botet, *Opt. Lett.* **21**, 1628 (1996); V. M. Shalaev, C. Douketis, T. Haslett, T. Stuckless, and M. Moskovits, *Phys. Rev. B* **53**, 11 193 (1996).
- ²⁵G. L. Fischer, R. W. Boyd, R. J. Gehr, S. A. Jenekhe, J. A. Osaheni, J. E. Sipe, and L. A. Weller-Brophy, *Phys. Rev. Lett.* **74**, 1871 (1995); R. J. Gehr, G. I. Fischer, R. W. Boyd, and J. E. Sipe, *Phys. Rev. A* **53**, 2792 (1996); R. W. Boyd, R. J. Gehr, G. L. Fischer, and J. E. Sipe, *Pure Appl. Opt.* **5**, 505 (1996), and references therein.
- ²⁶K. W. Yu, *Phys. Rev. B* **49**, 9989 (1994).
- ²⁷C. Zhang, X. Wu, S. Wu, and W. Su, *Phys. Rev. B* **54**, 16 349 (1996).
- ²⁸R. Rossignol, D. Ricard, K. C. Rustagi, and Flytzanis, *Opt. Commun.* **55**, 1413 (1985).
- ²⁹G. R. Olbright, N. Peyghambarian, S. W. Koch, and L. Banyai, *Opt. Lett.* **12**, 413 (1987).
- ³⁰D. Stroud and X. Zhang, *Physica A* **207**, 55 (1994); X. Zhang and D. Stroud, *Phys. Rev. B* **49**, 944 (1994).
- ³¹D. J. Bergman, E. Duering, and M. Murat, *J. Stat. Phys.* **58**, 1 (1990).
- ³²F. Brouers, S. Blacher, and A. K. Sarychev, in *Fractals in the Natural and Applied Sciences* (Chapman and Hall, London, 1995), Chap. 24.
- ³³F. Brouers, A. K. Sarychev, S. Blacher, and O. Lothaire, *Physica A* **241**, 146 (1997).
- ³⁴F. Brouers, S. Blacher, A. N. Lagarkov, A. K. Sarychev, P. Gadenne, and V. M. Shalaev, *Phys. Rev. B* **55**, 13 234 (1997).
- ³⁵A. N. Lagarkov, K. N. Rozanov, A. K. Sarychev, and A. N. Simonov, *Physica A* **241**, 199 (1997).
- ³⁶P. Gadenne, F. Brouers, V. M. Shalaev, and A. K. Sarychev, *J. Opt. Soc. Am. B* **15**, 68 (1998).
- ³⁷D. A. G. Bruggeman, *Ann. Phys. (Leipzig)* **24**, 636 (1935).
- ³⁸X. C. Zeng, D. J. Bergman, P. M. Hui, and D. Stroud, *Phys. Rev. B* **38**, 10 970 (1988); X. C. Zeng, P. M. Hui, D. J. Bergman, and D. Stroud, *Physica A* **157**, 10 970 (1989).
- ³⁹D. J. Bergman, in *Composite Media and Homogenization Theory*, edited by G. Dal Maso and G. F. Dell'Antinio (Birkhauser, Boston, 1991), p. 67.
- ⁴⁰O. Levy and D. J. Bergman, *J. Phys.: Condens. Matter* **5**, 7095 (1993).
- ⁴¹K. P. Yuen, M. F. Law, K. W. Yu, and P. Sheng, *Phys. Rev. E* **56**, R1322 (1997); H. Ma, R. Xiao, and P. Sheng, *J. Opt. Soc. Am. B* **15**, 1022 (1998); H. C. Lee, K. P. Yuen, and K. W. Yu, *Phys. Rev. B* **51**, 9317 (1995).
- ⁴²W. M. V. Wan, H. C. Lee, P. M. Hui, and K. W. Yu, *Phys. Rev. B* **54**, 3946 (1996).
- ⁴³P. M. Hui, P. Cheung, and Y. R. Kwong, *Physica A* **241**, 301 (1997), and references therein.
- ⁴⁴P. M. Hui and D. Stroud, *Phys. Rev. B* **49**, 11 729 (1994).
- ⁴⁵A. K. Sarychev and A. P. Vinogradov, *J. Phys.: Condens. Matter* **14**, L487 (1981); Y. Gefen, A. Aharony, B. B. Mandelbrot, and S. Kirkpatrick, *Phys. Rev. Lett.* **47**, 1771 (1981); A. P. Vinogradov and A. K. Sarychev, *Zh. Éksp. Teor. Fiz.* **85**, 1144 (1983) [*Sov. Phys. JETP* **58**, 665 (1983)]; B. B. Mandelbrot and J. Given, *Phys. Rev. Lett.* **52**, 1853 (1984); L. de Arcangelis, S. Redner, and A. Coniglio, *Phys. Rev. B* **31**, 4725 (1985).
- ⁴⁶*Introduction to Percolation Theory*, 2nd ed., by D. Stauffer and A. Aharony (Taylor and Francis, Philadelphia, 1991).
- ⁴⁷G. A. Niklasson and C. G. Granqvist, *J. Appl. Phys.* **55**, 338 (1984).
- ⁴⁸Y. Yagil, P. Gadenne, C. Julien, and G. Deutscher, *Phys. Rev. B* **46**, 250 (1992).
- ⁴⁹T. W. Noh, P. H. Song, Sung-Il Lee, D. C. Harris, J. R. Gaines, and J. C. Garland, *Phys. Rev. B* **46**, 421 (1992).
- ⁵⁰P. Gadenne, A. Beghadi, and J. Lafait, *Opt. Commun.* **65**, 1 (1988).
- ⁵¹P. Gadenne, Y. Yagil, and G. Deutscher, *J. Appl. Phys.* **66**, 301 (1989).
- ⁵²Y. Yagil, M. Yosefin, D. J. Bergman, G. Deutscher, and P. Gadenne, *Phys. Rev. B* **43**, 1134 (1991).
- ⁵³J. C. Maxwell Garnett, *Philos. Trans. R. Soc. London* **203**, 38 (1904).
- ⁵⁴F. Brouers, J. P. Clerc, and G. Giraud, *Phys. Rev. B* **44**, 5299 (1991); F. Brouers, J.M. Jolet, G. Giraud, J. M. Laugier, and Z. A. Randriamanantany, *Physica A* **207**, 100 (1994).
- ⁵⁵A. P. Vinogradov, A. M. Karimov, and A. K. Sarychev, *Zh. Éksp. Teor. Fiz.* **94**, 301 (1988) [*Sov. Phys. JETP* **67**, 2129 (1988)].
- ⁵⁶G. Depardieu, P. Frioni, and S. Berthier, *Physica A* **207**, 110 (1994).
- ⁵⁷A. K. Sarychev, D. J. Bergman, and Y. Yagil, *Physica A* **207**, 372 (1994); *Phys. Rev. B* **51**, 5366 (1995); R. Levy-Nathansohn and D. J. Bergman, *Physica A* **241**, 166 (1997); *Phys. Rev. B* **55**, 5425 (1997).
- ⁵⁸S. I. Bozhevolnyi, I. I. Smolyaninov, and A. V. Zayats, *Phys. Rev. B* **51**, 17 916 (1995).
- ⁵⁹M. Moskovits, *Rev. Mod. Phys.* **57**, 783 (1985); *Surface Enhance Raman Scattering*, edited by R. K. Chang and T. E. Furtak (Plenum, New York, 1982); M. I. Stockman, V. M. Shalaev, M. Moskovits, R. Botet, and T. F. George, *Phys. Rev. B* **46**, 2821 (1992).
- ⁶⁰J. Plon, M. Gadenne, P. Gadden, C. Sella, C. Naud, and C. Julien, *Physica A* **241**, 183 (1997).
- ⁶¹F. Brouers, J. P. Clerc, G. Giraud, J. M. Laugier, and Z. A. Randriamanantany, *Phys. Rev. B* **47**, 666 (1993).
- ⁶²A. M. Dykhne, *Zh. Éksp. Teor. Fiz.* **59**, 110 (1970) [*Sov. Phys. JETP* **32**, 348 (1971)].
- ⁶³E. Betzig *et al.*, *Science* **257**, 189 (1992).
- ⁶⁴D. J. Frank and C. J. Lobb, *Phys. Rev. B* **37**, 302 (1988).
- ⁶⁵A. K. Sarychev, D. J. Bergman, and Y. Strelniker, *Phys. Rev. B* **48**, 3145 (1993).
- ⁶⁶L. Tortet, J. R. Gavarrí, J. Musso, G. Nihoul, J. P. Clerc, A. N.

- Lagarkov, and A. K. Sarychev, Phys. Rev. B (to be published).
- ⁶⁷P. J. Reynolds, W. Klein, and H. E. Stanley, J. Phys.: Condens. Matter **10**, L167 (1977).
- ⁶⁸A. K. Sarychev, Condens. Matter Zh. Éksp. Teor. Fiz. **72**, 1001 (1977) [Sov. Phys. JETP **45**, 524 (1977)].
- ⁶⁹J. Bernasconi, Phys. Rev. B **18**, 2185 (1978).
- ⁷⁰A. Aharony, Physica A **205**, 330 (1994).
- ⁷¹*Hand book of Optical Constants of Solids*, edited by E. D. Palik (Academic, New York, 1985); P. B. Johnson and R. W. Christy, Phys. Rev. B **6**, 4370 (1972).
- ⁷²R. W. Boyd, *Nonlinear Optics* (Academic, New York, 1992); L. D. Landau, E. M. Lifshits, and L. P. Pitaevskii, *Electrodynamics of Continuous Media*, 2nd ed. (Pergamon, Oxford, 1984).
- ⁷³G. I. Stegeman, M. Sheik-Bahae, E. W. Van Stryland, and As-santo, Opt. Lett. **18**, 13 (1993).